Cell Communication and Signaling

RESEARCH

Open Access

Exercise-conditioned plasma ameliorates postoperative cognitive dysfunction by activating hippocampal cholinergic circuit and enhancing BDNF/TrkB signaling

Xiaodi Lu[1†], Weijie Xiong[2†], Zhuo Chen[1], Yurou Li[2], Fengyan Xu[2], Xue Yang[2], Meiwen Long[2], Wenhan Guo[2], Shuliang Wu[2*], Liang Sun[2*] and Guonian Wang[3*]

Abstract

Background Postoperative cognitive dysfunction (POCD) is a prevalent complication following anesthesia and surgery, particularly in the elderly, leading to increased mortality and reduced quality of life. Despite its prevalence, there are no effective clinical treatments. Exercise has shown cognitive benefits in aging and various diseases, which can be transferred to sedentary animals through plasma. However, it is unclear if exercise-conditioned plasma can replicate these benefits in the context of POCD.

Methods Sixteen-month-old male C57BL/6J mice underwent 30 days of voluntary running wheel training or received systemic administration of exercise-conditioned plasma, followed by tibial fracture surgery under general anesthesia at 17 months of age. Cognitive performance, hippocampal synaptic deficits, neuroinflammation, BDNF/TrkB signaling, and medial septum (MS)-hippocampal cholinergic activity were evaluated through immunohistochemical staining, transmission electron microscopy, Western blotting, and biochemical assays. To investigate the role of hippocampal BDNF signaling and cholinergic activity in the therapeutic effects, the TrkB antagonist ANA-12 and the cholinergic receptor muscarinic 1 (CHRM1) antagonist trihexyphenidyl (THP) were administered via intraperitoneal injection, and adeno-associated virus (AAV) vectors expressing *Chrm1* shRNA were delivered via intrahippocampal stereotaxic microinjection.

Results Exercise-conditioned plasma mimicked the benefits of exercise, alleviating cognitive decline induced by anesthesia/surgery, restoring hippocampal synapse formation and levels of regulators for synaptic plasticity, inhibiting neuroinflammatory responses to surgery by microglia and astrocytes, augmenting BDNF production

†Xiaodi Lu and Weijie Xiong contributed equally to this work.

*Correspondence:
Shuliang Wu
wushuliang@ems.hrbmu.edu.cn
Liang Sun
sunliang@hrbmu.edu.cn
Guonian Wang
wangguonian609cn@aliyun.com

Full list of author information is available at the end of the article

and TrkB phosphorylation in hippocampal neurons, astrocytes, and microglia, upregulating MS expression of choline acetyltransferase (CHAT) and hippocampal expression of CHRM1 in neurons and astrocytes, and enhancing hippocampal cholinergic innervation and acetylcholine release. Conversely, ANA-12 administration blocked TrkB activation and reduced the protective effects on cognition, synaptic deficits, and neuroinflammatory reactivity of glial cells post-surgery. Similarly, THP administration or intrahippocampal delivery of AAV-*Chrm1* shRNA inhibited the activation of the hippocampal cholinergic circuit by exercise plasma, negating the cognitive and neuropathological benefits and reducing BDNF/TrkB signaling enhancements.

Conclusion Exercise-conditioned plasma can replicate the protective effects of exercise against anesthesia/surgery-induced neuroinflammation, synaptic, and cognitive impairments, at least partly, through CHRM1-dependent regulation of hippocampal cholinergic activity and BDNF/TrkB signaling.

Keywords POCD, Exercise, Plasma, Cholinergic circuit, BDNF/TrkB

Background

Postoperative cognitive dysfunction (POCD) is a common complication following anesthesia and surgery, characterized by a decline in various cognitive domains, including attention, learning, memory, information processing, and execution, alongside increased confusion and anxiety [1–3]. POCD can persist for weeks, months, or even years after surgery, leading to prolonged hospitalization, decreased quality of life, and increased mortality among affected patients [4–6]. POCD occurs in approximately 10-54% of individuals undergoing anesthetic and surgical procedures, with a pooled incidence of 29% reported in clinical studies [7, 8]. The causes of POCD are not fully understood. Age is the most established risk factor, with elderly patients (≥65 years) being more susceptible to POCD [8].

Neuroinflammation is widely recognized as a major contributor to POCD, driven by anesthesia/surgery-induced systemic inflammatory mediators such as blood-brain barrier-permeable cytokines (TNFα, IL-1β, IL-6, etc.) [9]. POCD-associated neuroinflammatory responses involve the aberrant activation of microglia and astrocytes. Microglia transform from their resting state as cerebral homeostasis-keepers and scavengers to a reactive state, producing and releasing inflammatory mediators [6, 10], while astrocytes shift from a neuroprotective phenotype involved in the regulation of neuronal activity and memory processing to a reactive state that may contribute to neuronal degeneration [11–14]. Neuronal dysfunction, considered secondary to neuroinflammation, is characterized by abnormal synapse structure and function, the fundamental units of neuronal communication and neural circuits. Specifically, synaptic plasticity, which underpins the dynamics of neuronal circuits and serves as a critical neurochemical foundation for learning and memory, is found to be impaired in the context of POCD [6, 15]. Brain-derived neurotrophic factor (BDNF), a well-established neurotrophin, exerts key modulatory effects on synaptic plasticity, neuronal excitability, and cognition via its receptor tropomyosin receptor kinase B (TrkB) [16]. Dysregulated BDNF/TrkB signaling is also implicated in the development of POCD [5, 17]. However, the interplay and causal relationships among these potential mechanisms mediating the pathogenesis of POCD remain to be determined. With the global population aging and the consequent rapid increase in the number of operations performed on the elderly, effective therapies to ameliorate POCD are desperately needed [15]. Despite attempts to target potential mechanisms of POCD in preclinical trials, there are currently no validated neurophysiologic biomarkers or effective preventive and therapeutic methods [1, 18], possibly due to the complex pathogenesis of POCD, where targeting a single mechanism is insufficient to reverse all pathological events.

Exercise is beneficial for improving health and cognitive functions in aging and disease states [19]. Regular exercise training significantly enhances cognitive performance in aging and Alzheimer's disease (AD) animal models [20] and alleviates both motor and cognitive impairments in Parkinson's disease (PD) models [21, 22]. Exercise also aids in recovery from cognitive impairments associated with frontotemporal degeneration [23], vascular dementia [24], and even disease treatments such as radiotherapy [25], chemotherapy [26], and surgery [15, 27], as reported by preclinical and clinical studies. The mechanisms underlying the cognitive benefits of exercise are not fully understood, but BDNF signaling is believed to play a crucial role [28]. Under physiological conditions, exercise activates the lactate/SIRT1/PCG1/FNDC5 pathway, enhancing hippocampal BDNF signaling, which mediates the enhancement of learning and memory functions [29]. In symptomatic mouse models of AD, hippocampal BDNF signaling is essential for exercise training to reverse cognitive deficits [30]. Clinical studies also use BDNF levels as indicators of exercise-related cognitive recovery [31]. Additionally, exercise-induced shifts in microglia and astrocytes from pro-inflammatory to anti-inflammatory phenotypes might contribute to cognitive protection. Exercise training leads to the phenotypes of

microglia and astrocytes towards neuroprotective and neurotrophic states, aiding cognitive function improvement in various cognitive impairment models, including AD [32, 33]. Remarkably, several rigorous studies highlight the role of blood plasma components in mediating the cognitive benefits of exercise. Plasma from exercise-trained elderly mice improves hippocampal neurogenesis and cognitive function in sedentary elderly mice, with liver-derived phospholipase Gpld1 identified as a key mediating factor [34]. Plasma from exercise-trained mice also reduces neuroinflammation and enhances memory recovery in AD models, with the complement pathway inhibitor clusterin playing a crucial role in these effects [35]. Exercise activates platelets to secrete platelet factor 4, promoting hippocampal neuroregeneration and cognitive improvement in aged mice [36]. The identification of various exercise-related cognitive-enhancing blood factors underscores the complexity of exercise effects, as evidenced by changes in the expression of over 200 secreted proteins across multiple tissues and cell types in model mice [37]. Nevertheless, whether exercise-conditioned blood/plasma can recapitulate the exercise-induced cognitive benefits under conditions of anesthesia and surgery remains to be determined.

In the adult mammalian brain, cholinergic projection neurons, which are involved in various cognitive functions such as attention, mood, and memory, primarily cluster in several subregions of the basal forebrain, including the medial septum (MS), diagonal band (DB), ventral pallidum, substantia innominata, and nucleus basalis [38]. Basal forebrain cholinergic neurons (BFCNs) act through G protein-coupled muscarinic acetylcholine (ACh) receptors (mAChRs); particularly cholinergic receptor muscarinic 1, CHRM1) and ionotropic nicotinic ACh receptors (nAChRs). BFCNs send extensive projections to the prefrontal cortex (PFC), the amygdala, and the hippocampus (HPC). Specifically, cholinergic neurons located in the MS and DB project to the HPC, broadly innervating all cornu ammonis (CA) regions, with the densest innervation detected in CA3 [39].

The MS- hippocampal circuit has long been proposed to regulate the encoding and consolidation of HPC-dependent memory [40]. An increase in hippocampal ACh release is observed during various memory tasks [41]. Blocking hippocampal mAChRs and α7 nAChRs through intrahippocampal infusion of cholinergic receptor antagonists or knocking out cholinergic receptors in excitatory neurons or interneurons results in abnormal cognitive outcomes in mice [42]. Additionally, positive allosteric modulation of CHRM1 enhances cognitive flexibility and effective salience in nonhuman primates [43]. Mechanistically, a surge of work implicates the basal forebrain cholinergic input in the sophisticated modulation of hippocampal network functions and synaptic plasticity. MS cholinergic neurons promote memory formation and consolidation by maintaining high hippocampal ACh levels through persistent firing during theta epochs [42, 44]. This activity suppresses aberrant network ripples, allows theta oscillations to dominate, and increases the signal-to-noise ratio during active exploration and rapid eye movement sleep. Endogenous cholinergic signaling reinforces hippocampal synaptic plasticity and long-term potentiation (LTP) by stabilizing GluA1 receptors on dendritic spines, facilitating learning-induced increases in the AMPA/NMDA receptor ratio, and enhancing axonal excitability in α7 nAChRs and CHRM1-dependent manners [45]. Furthermore, hippocampal cholinergic activity preserves contextual memory by activating BDNF signaling via astrocytic CHRM1 in mice [46].

Dysfunction of the basal forebrain- hippocampal cholinergic circuit is implicated in the development of multiple neurodegenerative and neuroinflammatory diseases, which could be promising therapeutic targets. Hippocampal cholinergic innervation is vulnerable to prion and AD-like pathology in mouse models. Enhancing hippocampal cholinergic signaling by allosteric activation of CHRM1 slows prion neurodegeneration and restores memory loss [47]. Photoactivating MS-HPC CA1 cholinergic inputs within a critical 3-hour time window during memory consolidation efficiently rescues tau-induced spatial memory deficits in a θ rhythm-dependent manner [48]. Pharmacological enhancement of cholinergic neurotransmission with cholinomimetic molecules alleviates the neuroinflammatory response of astrocytes and microglia, sustains hippocampal synapses, and improves cognitive outcomes in an AD mouse model [49]. The MS-hippocampal cholinergic neurotransmission is impaired in mice with sepsis, whereas selective optogenetic/chemogenetic activation of hippocampal cholinergic innervation alleviates defects in synaptic plasticity and memory [50], implying potential protective effects of hippocampal cholinergic activity under systemic inflammation-induced central neuroinflammatory conditions. Consistently, surgery-induced delirium in mice manifests as reduced hippocampal ACh release and impaired LTP and synaptic plasticity induced by high-frequency burst stimulation [12]. These impairments can be reversed by normalizing ACh release with galantamine. Furthermore, the hippocampal cholinergic network might benefit from exercise and blood factors in aging and neurodegenerative models. Regular exercise not only leads to the re-emergence of the MS cholinergic/nestin neuronal phenotype and the restoration of hippocampal ACh efflux and spatial behavior in an nerve growth factor-dependent manner in a thiamine deficiency rat model [51, 52] but also reverses age-related declines in rat hippocampal cholinergic fibers and neurocognitive behaviors [53].

Our previous study reveals that blood from young mice (3-month-old) restores mouse hippocampal cholinergic activity and improves AD-like pathology and cognitive disorder [54]. However, it remains unclear whether exercise-conditioned blood/plasma can reverse the postoperative MS-hippocampal cholinergic defect and what role hippocampal cholinergic activation plays in the protective effects of exercise plasma under anesthetic/surgical conditions.

Based on the above background information, we hypothesized that exercise-conditioned plasma might attenuate POCD, which may be mediated by the activated hippocampal cholinergic circuit and enhanced BDNF/TrkB signaling. To test this hypothesis, we established a POCD model using aged mice by canonical tibia fracture surgery under anesthesia, treated the model mice with voluntary exercise or exercise-conditioned plasma, and measured cognition, synaptic deficits, neuroinflammation, BDNF/TrkB signaling, and cholinergic activity. The mediation of cholinergic activity and BDNF/TrkB transduction for the therapeutic effects of exercise plasma was determined by pharmacological antagonism and in vivo silencing.

Materials and methods

Animals and experimental designs

Adult C57BL/6J mice were purchased from Beijing Vital River Laboratory Animal Technology Co., Ltd. (China), housed on SPF conditions under a 12-hour light/dark cycle, with temperature maintained at 21–24 °C and humidity at 40-60%, and had ad libitum access to sterilized food and water. All animal handling and use were approved by Institutional Research Board of Harbin Medical University (No. HMUIRB2023016) and performed in strict compliance with the Laboratory animal—Guideline for ethical review of animal welfare (GB/T 35892−2018) and the Animal Research: Reporting of In Vivo Experiments (ARRIVE) guidelines 2.0.

Aged male C57BL/6J mice (16-month old) at the beginning of each experiment were mainly randomized into: Control (Con), Surgery (Sur), Exercise (Ex)+Sur, Exercise Plasma (ExP)+Sur, ANA12+ExP+Sur, Trihexyphenidyl hydrochloride (THP)+ExP+Sur, negative control (NC)+ExP+Sur, and shRNA+ExP+Sur groups. Two separate cohorts of animals (n=6/group/cohort) were used for each experimental condition: one (Cohort 1) for immunohistochemistry (IHC) and another (Cohort 2) for molecular biological, biochemical, and ultrastructural analyses. All groups except Con underwent POCD model surgery under anesthesia at 17 months of age, following a 30-day intervention period. The Ex+Sur group were subjected to voluntary exercise in a running wheel 30 days before surgery, while the ExP+Sur, ANA12+ExP+Sur, THP+ExP+Sur, NC+ExP+Sur, and shRNA+ExP+Sur groups were administered with the exercised mice-derived plasma during the same period. Mice in the ANA12+ExP+Sur and THP+ExP+Sur groups underwent intraperitoneal (*i.p.*) injection of ANA-12 (0.5 mg/kg; diluted to 0.125 mg/mL in saline from a 5 mg/mL stock solution in dimethyl sulfoxide (DMSO); S7745; Selleck, Shanghai, China) and THP (1 mg/kg; diluted to 0.25 mg/mL in saline from a 10 mg/mL stock solution in DMSO; S4542; Selleck) 30 min prior to plasma administration, respectively. Mice in the Con, Sur, Ex+Sur and ExP+Sur groups were intraperitoneally injected with equal amount of the vehicle solution at the same time. To further investigate potential off-target effects, additional groups were included: ANA12+Ex+Sur and THP+Ex+Sur, where exercise-trained POCD model mice were treated with ANA12 or THP, respectively, at the same dosage and time points as the ANA12+ExP+Sur and THP+ExP+Sur groups. The shRNA+ExP+Sur and NC+ExP+Sur groups received intrahippocampal microinjections of adeno-associated virus (AAV) vectors containing *Chrm1* shRNA and NC shRNA sequences 2 days prior to the beginning of plasma administration, respectively. Cognitive tests including open field (OF), novel location recognition (NLR), novel object recognition (NOR), and Y maze tests were conducted from 3 days to 6 days post surgery, with one test performed each day (Figs. 1A, 5A, 8A and 10A, S6A and S9A). Animals were euthanized immediately 30 min after the end of all behavioral tests, and brain tissues were collected for subsequent histopathological, biochemical or molecular biological assays.

Running paradigms

The mice in the Ex+Sur group and the exercise plasma donor mice were subjected to voluntary exercise training on running wheels for 30 days, according to the previously described protocols with minor modifications [30, 55]. The running wheel (21 cm in diameter and 8 cm in width) is made of stainless-steel frames and transparent plastic panels and equipped with a magnetic induction counter to monitor the exercise intensity. Each mouse singly spent 3 h in the running wheels daily and was returned to the original cages for the remaining 21 h until the completion of the exercise training period. The daily running distance was recorded for each mouse to assess exercise performance.

Plasma collection and systemic administration

Plasma was collected and administered following previously reported procedures with slight modifications [34–36]. After completing a 30-day exercise training regimen on running wheels, the plasma donor mice were anesthetized with 1% pentobarbital sodium (50 mg/kg). Blood was obtained from right ventricle via intracardial

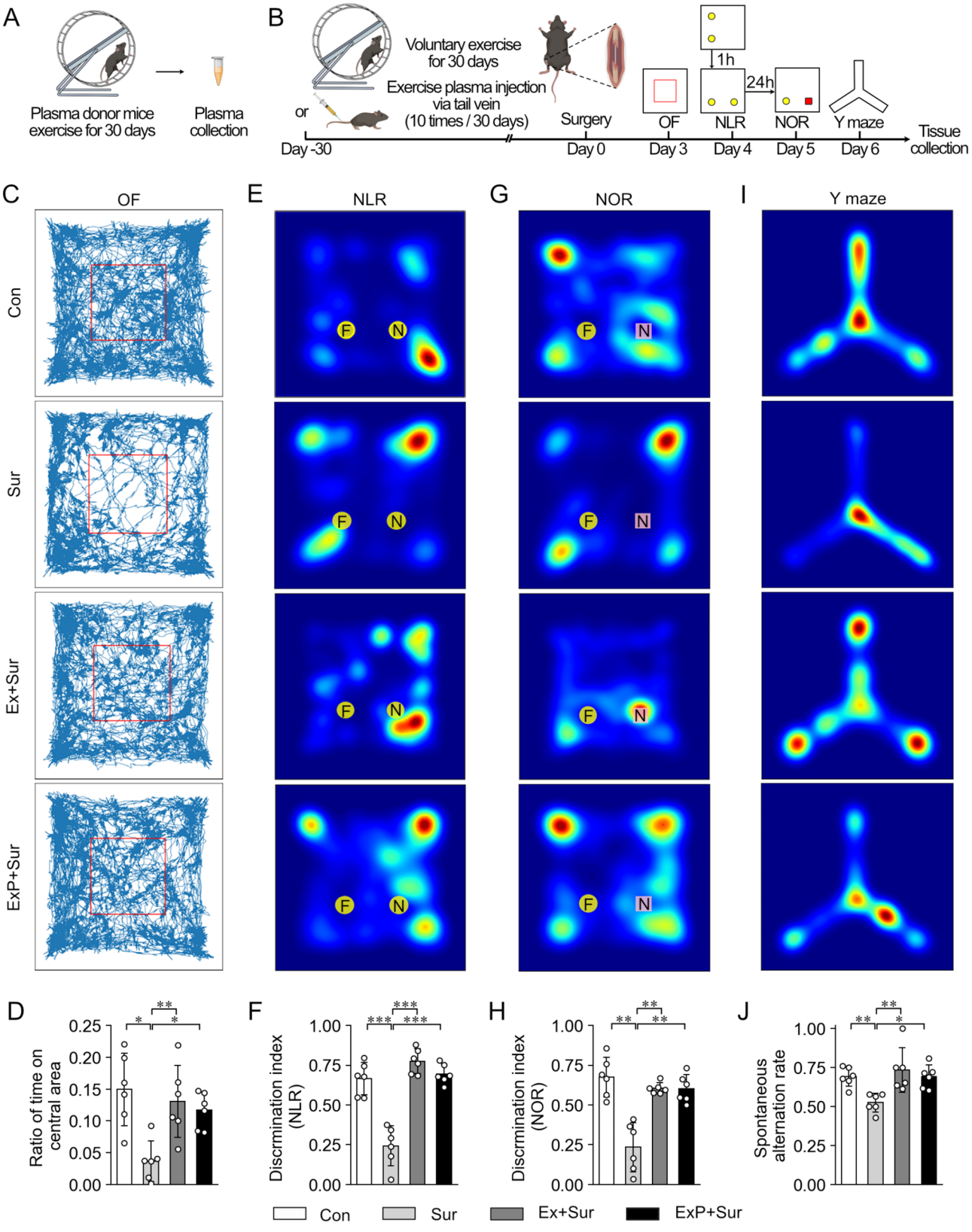

Fig. 1 Exercise-conditioned plasma mimicked the beneficial effects of exercise on postoperative cognitive impairment. (**A**-**B**) Schematic illustration of the collection of exercise plasma (**A**) and the experimental design of exercise training, exercise plasma injection, surgery, cognitive tests and tissue collection (**B**). (**C**-**D**) Representative locus diagrams and the statistical analyses of the OF tests. (**E**-**J**) Representative trajectory heat maps and the related statistical analyses of the NLR (**E**, **F**), NOR (**G**, **H**) and Y maze tests (**I**, **J**). Data are expressed as mean ± SD; $n = 6$ per group; * $P < 0.05$, ** $P < 0.01$, *** $P < 0.001$

bleeding using a Vacutainer Lithium Heparin Tube (367884; BD; New Jersey, USA), and then centrifugated at 1000 g, 4 °C for 15 min. The plasma was pooled together, aliquoted and stored at −80 °C until required. Systemic administration of plasma was conducted through intravenous tail vein injection at a dose of 100 μL per injection. The administration of every batch of mice was scheduled at the same time period, once every 3 days, and administrated 10 times over a period of 30 days.

Stereotaxic microinjections of AAV vectors

Stereotaxic microinjections of AAV vectors were conducted following the established protocols [50, 56]. Mice were anesthetized by *i.p.* injection of 1% pentobarbital sodium (50 mg/kg) and secured on a stereotaxic frame. The scalp was shaved, sterilized with povidone-iodine plus 75% ethanol, and locally anesthetized with compound lidocaine cream (2.5% lidocaine and 2.5% prilocaine; H20063466; TONGFANG PHARMACEUTICAL CROUP CO., LTD; Beijing, China). A sagittal incision was made, and craniotomies (1–2 mm in diameter) were created above the bilateral parietal cortex and HPC using a high-speed drill. Viral injections into the hippocampal CA1 region were performed using a Hamilton microliter syringe (2.5 μL) with 33-gauge Small Hub RN Needle attached to the stereotaxic apparatus. Each side of the hippocampal tissue received a single-site viral injection. The injections were targeted at the following stereotaxic coordinates: anteroposterior (AP) -2.3 mm from the bregma, mediolateral (ML) ± 2.0 mm from the midline, and dorsoventral (DV) -1.5 mm from the pial surface. A volume of 0.5 μL/site of AAV vectors was injected at a rate of 50 nL/min. The micropipette was withdrawn slowly 10 min after the injection. Surgical wounds were disinfected with povidone-iodine plus 75% ethanol, and local analgesia was provided with compound lidocaine cream. Mice were kept on a heating pad at 37 °C until they recovered from anesthesia. The POCD surgery and subsequent experiments were carried out in 30 days post injection of AAV vectors. The AAV vectors used in this study were synthesized by Obio Technology (shanghai) Corp Ltd (Shanghai, China), and included: AAV2/5-*U6-Chrm1* shRNA-CMV-EGFP-WPRE (TargetSeq: ATCAAGATGCCTATGGTAGAT) and AAV2/5-*U6*-NC shRNA-CMV-EGFP-WPRE (TargetSeq: CCTAAGGTTAAGTCGCCCTCG). Both AAV vectors had titers of ≥1.0E+12 v.g./mL.

Anesthesia and surgery

The surgery to establish the POCD model was performed according to published protocols, using 1% pentobarbital sodium (50 mg/kg, *i.p.*) to induce general anesthesia, which lasted for at least 40 min [3]. The right hind limb of mice was shaved and disinfected using povidone-iodine plus 75% ethanol. A skin incision was made along the medial aspect of the right hind limb to expose the midshaft of the tibia and visualize the tibial plateau. A 0.5-mm hole was drilled through the tibial plateau into the intramedullary canal using a 25-gauge needle, followed by the insertion of an intramedullary needle (a 0.38-mm stainless steel pin) into the medullary cavity. Subsequently, the tibia midshaft was fractured using straight Bonn scissors, and the stabilization of the fracture sight was assessed. Surgical wounds were sutured and disinfected with povidone-iodine plus 75% ethanol, and local analgesia was administered with compound lidocaine cream. Mice were allowed to recover on a heating pad (at 37 °C) and then returned to clean home cages.

OF

To assess the general learning and exploratory activity and the anxiety-like behavior of mice, OF test was performed in an opaque white plastic OF chamber (40×40×40 cm^3). During test phase, each mouse was placed in the central area of arena and allowed to explore freely for 30 min [57, 58]. Animal behavior was recorded by a digital camera mounted right above the chamber. The ratio of time each mouse spent on the central zone was calculated. Entry into the central zone was defined as the moment when all four paws of the mouse crossed the boundary into this area. The arena was cleaned with 75% ethanol between each test to eliminate odor cues.

NLR and NOR

To evaluate the HPC-dependent spatial reference memory and memory retention, the NLR and NOR tasks were conducted in the OF chamber following modified protocols based on previous studies [34, 36, 59]. Mice were habituated to the arena through the OF task. In the training phase, 24 h post OF test, mice were placed in the center of the arena with 2 identical objects (yellow wood cones: 4.5 cm in base diameter, 7.5 cm in height) positioned 10 cm away from the walls. They were given 10 min to freely explore the arena and objects. Subsequently, during the NLR task testing phase (1 h after training), one of the familiar objects was relocated to the opposite corner, and mice was allowed another 10-minute exploration session. In the NOR task testing phase (24 h later), the displaced familiar object was replaced with a novel object (red wood cube with sides of 5 cm), and mice were placed in the arena center for a 10-minute exploration period. Each session was recorded by a digital camera. Exploration was defined as the mouse directly attending to the object with its head positioned within 2–3 cm of the object, accompanied by active vibrissae sweeping or sniffing [60, 61]. To ensure objectivity, researchers were blinded to the experimental conditions during the scoring process. The following measurements

were calculated: Discrimination index (NLR) = novel location exploration time/ total exploration time; Discrimination index (NOR) = novel object exploration time/ total exploration time. Thorough cleaning of the arena and objects with 75% ethanol was performed between each session.

Y maze

Y maze spontaneous alternation test was conducted to evaluate the short-term spatial working memory of mice [30]. The Y maze was made of opaque white acrylic resin, and consisted of 3 identical arms (30 cm-long, 6 cm-width and 15 cm-high), 120° apart from each other. Mice was placed in one arm and allowed to freely explore through the Y maze during an 8-min test session, which was videoed by a digital camera. The numbers and sequences of arm entries were recorded. An arm entry was defined as the moment when all four paws of the mouse cross the threshold from the central zone into the arm, with the animal's snout oriented toward the end of the arm. The alternation was defined as consecutive entries into all three arms, and the spontaneous alternation rate was calculated as: number of actual alternations / (total number of arm entries −2). The Y maze was cleaned thoroughly with 75% ethanol between tests.

Tissue collection

For Cohort 1, mice were anesthetized with 1% pentobarbital sodium (50 mg/kg) and transcardially perfused with ice-cold PBS (pH 7.4). The whole brain was removed, fixed in 4% paraformaldehyde in PBS (pH 7.4) for 48 h at 4 °C before the procedures of immunohistochemical staining. For Cohort 2, animals were euthanized as described for Cohort 1. The fresh HPC was dissected rapidly. A small tissue sample (1×1×1 mm^3) microdissected from the CA1 region of one hemisphere was fixed using 2.5% glutaraldehyde plus 4% paraformaldehyde in 0.1 M sodium cacodylate buffer for transmission electron microscopy (TEM) analysis. The remaining tissue from this hemisphere and the entire contralateral hemisphere were snap-frozen in liquid nitrogen and stored at -80 °C for ACh assay and Western blotting.

Immunohistochemistry

Tissue processing and IHC was conducted on paraffin sections following standard protocols. The paraffin-embedded brains were coronally sectioned at 4 μm using a microtome (HistoCore NANOCUT R, Leica; Wetzlar, Germany). For immunofluorescence (IF) staining, the sections were dewaxed and hydrated, and washed with 0.01 M PBS (pH 7.4) containing 0.01% Tween-20 (PBST), which served as the washing buffer for all the IHC washing steps. Antigen retrieval was carried out using sodium citrate buffer (pH 6.0) in a pressure cooker at full pressure for 3 min. Subsequently, the sections were blocked in 5% BSA in PBST for 1 h, followed by overnight incubation with the primary antibodies (as listed in Table S1) in the blocking solution at 4 °C. This was followed by incubation with corresponding fluorescein-conjugated secondary antibodies (as listed in Table S2) at 37 °C in the dark for 1 h. The sections were then counterstained with DAPI (1 μg/mL; Sigma-Aldrich, Merck Millipore; MA, USA) for 5 min and mounted in 50% glycerol-PBS. Fluorescence images were captured under a fluorescence microscope (BX51, Olympus; Tokyo, Japan). For HRP-DAB staining for CHAT, endogenous peroxidases were blocked using with 3% H_2O_2 at room temperature for 10 min following antigen retrieval. After blocking, the sections were incubated overnight with goat anti-CHAT (1:200; AB144P; Sigma-Aldrich, Merck Millipore) in blocking solution at 4 °C, followed by incubation with HRP-conjugated rabbit anti-goat IgG H+L (1:200; abs20005; Absin) at 37 °C for 1 h [62]. This was succeeded by a 30-minute incubation in freshly prepared DAB working solution (P0203; Beyotime, Shanghai, China), counterstaining with 0.1% Mayer hematoxylin, dehydration in ethanol and xylene, and mounting in neutral resin. The HRP-DAB-stained sections were photographed using a Leica DM4 B microscope equipped with Leica DMC5400 camera.

TEM

After being fixed in a solution of 2.5% glutaraldehyde and 4% paraformaldehyde for over 24 h, the hippocampal tissue samples (1×1×1 mm^3) microdissected from the CA1 region underwent a postfixation step in 1% osmic acid and 1.5% potassium ferrocyanide for 2 h. Subsequently, they were dehydrated in a gradient of ethanol and acetone, immersed, and embedded in epoxy resin before being sectioned into 70-nm thick ultrathin slices. These sections were then transferred onto copper grids, stained with a mixture of 3% uranyl acetate and lead citrate, and examined using an HT7700 transmission electron microscope (Hitachi; Osaka, Japan).

Western blotting

For Western blotting (WB) analysis, brain tissues were homogenized in RIPA lysis buffer (P0013K; Beyotime) supplemented with 1% PMSF (ST506; Beyotime) and 1% phosphatase inhibitor cocktail (B15001; Selleck). The protein concentration was measured using BCA Protein Assay Kit (P0012; Beyotime). Subsequently, the protein samples were mixed with 5× loading buffer (P0015; Beyotime), resolved by SDS polyacrylamide gel electrophoresis using a running buffer (25 mM Tris, 190 mM Glycine, 0.1% SDS), and then electroblotted onto polyvinylidene difluoride (PVDF) membranes (Merck Millipore) using a transfer buffer (25 mM Tris, 190 mM Glycine, 0.1% SDS, 20% Methanol). After thorough washing with 1 ×

Tris-buffered saline with 0.1% Tween-20 (TBST), which was used for all washing steps in WB, the PVDF membranes were blocked with 5% skim milk in TBST at room temperature for 1 h. Following this, the membranes were incubated with the primary antibodies (as listed in Table S1) in the blocking solution at 4 °C overnight, and then with the corresponding HRP-conjugated secondary antibodies (as listed in Table S2) in the blocking solution at 37 °C for 1 h. The protein signals were developed with ECL kit (P0018FS; Beyotime) and visualized using the Tanon 4600 chemiluminescence image analysis system (Tanon; Shanghai, China).

ACh assay

The frozen HPC tissues were homogenized (10% (w/v)) on ice in PB (50 mM, pH7.4) and centrifugated at 1000 g, 4 °C for 10 min. The supernatant was collected and used for ACh concentration determination using Amplex™ Acetylcholine/Acetylcholinesterase Assay Kit (A12217, Thermo Fisher Scientific; MA, USA) in accordance with the manufacturer's instructions. The emission fluorescence at 590 nm of reaction system stimulated by the 560-nm excitation light was measured using an SpectraMax M2 microplate reader (Molecular Devices Corporation; CA, USA). The ACh level was calculated by the standard curve and expressed as μmol per mg tissue protein.

Data processing and statistical analyses

Videos of behavioral tests were analyzed by the Animapp software [63], and visualized by the Seaborn library in Python environment. IF/IHC images, TEM images, and Western blots were processed and analyzed using the Fiji.app/Image J software. All the quantitative analyses were performed by the investigators blind to the related experimental conditions. For IF staining, the fluorescence intensity of synaptophysin (SYP; a presynaptic marker of synaptic vesicles), postsynaptic density protein 95 (PSD-95; a scaffolding protein located at excitatory synapses), phosphorylated cAMP response element-binding protein (CREB) (p-CREB), c-fos, glial fibrillary acidic protein (GFAP), complement component 3 (C3), ionized calcium-binding adapter molecule 1 (IBA1), inducible nitric oxide synthase (iNOS), BDNF, p-TrkB (Tyr816), and CHRM1 was measured in the CA1 area of the hippocampus, the primary region of interest. Colocalization analyses in the CA1 region were performed using the Coloc 2 plugin of Fiji.app/Image J software, calculating the Pearson correlation coefficients and Manders coefficients for C3 with GFAP, iNOS with IBA1, BDNF with NeuN, GFAP or IBA1, p-TrkB (Tyr816) with NeuN, GFAP or IBA1, and CHRM1 with NeuN or GFAP. CHAT fluorescence intensity was primarily measured in the medial septum. For HRP-DAB staining, the integrated intensity of CHAT was measured in the CA3 area of the hippocampus. In the TEM images of the CA1 region, synapses were identified by the presence of presynaptic vesicles and characteristic postsynaptic density using the Wand tool of Fiji.app/Image J software and quantified manually. For Western blot analyses, the integrated density of the target protein blots was measured and normalized to that of β-actin, which served as the internal loading control, to account for variations in protein loading and transfer efficiency. Schematics were generated using Medpeer.cn and Affinity Photo 2 software.

Data were expressed as mean ± standard deviation (SD). Statistical analyses were performed using the Pingouin library and visualized using the Seaborn library in Python environment. The comparisons of means between two groups were conducted using independent Student's *t*-test (two-tailed). The between-group comparisons of means from multiple groups were analyzed using one-way analysis of variance (ANOVA) followed by post hoc Bonferroni's multiple comparison test. $P<0.05$ was considered statistically significant.

Results

Systemic plasma administration mimics the beneficial effects of exercise on postoperative cognitive decline

To assess the efficacy of exercise and plasma from exercised mice in counteracting deficits in hippocampal-dependent learning and memory induced by anesthesia/surgery, we conducted the OF, NLR, NOR and Y maze tests sequentially from days 3 to 6 post-surgery (Fig. 1A-B). To rule out potential confounding effects of surgery on motor performance, we analyzed the average velocity of mice during the OF test, which showed no significant differences between groups (Fig.S1). In the OF test (Fig. 1C-D), aged mice (17 months old) in the Surgery (Sur) group, subjected to a standard POCD model surgery (tibia fracture) without any treatment, showed a significant decrease in time spent in the central zone of the OF arena ($P<0.05$) compared to the Con group. This reduction indicates a lower exploratory drive and learning propensity, along with increased anxiety-like behavior levels. In contrast, aged mice in the Ex + Sur group, which had engaged in a 30-day voluntary exercise regimen on a running wheel before surgery ($P<0.01$ vs. Sur), and those in the ExP + Sur group, which received systemic infusions of exercise-conditioned plasma instead of physical exercise for 30 days pre-surgery, exhibited normalized exploratory behavior in the central zone and decreased anxiety-like behavior ($P<0.05$ vs. Sur). The NLR and subsequent NOR tests conducted 24 h later (Fig. 1E-H), showed that the Sur group spent less time with objects in novel locations and with novel objects (*P* values < 0.01 vs. Con), suggesting impaired spatial reference memory and retention [34, 36, 59]. Conversely, the Ex + Sur group

displayed a preference for the relocated and novel objects (*P* values < 0.01 vs. Sur), and the ExP + Sur group showed similar recovery in discriminating locations and objects (*P* values < 0.01 vs. Sur). During the Y maze test (Fig. 1I-J), the Sur group exhibited a reduced spontaneous alternation frequency compared to the Con group ($P < 0.01$), indicating a negative effect on spatial working memory attributable to anesthesia and surgery [30]. In comparison, both the Ex + Sur ($P < 0.01$ vs. Sur) and ExP + Sur groups ($P < 0.05$ vs. Sur) showed significant improvements in spontaneous alternation behavior and working memory. Collectively, these behavioral test results suggest that tibia fracture surgery under anesthesia leads to impairments in HPC-dependent cognitive domains in aged mice. Furthermore, systemic administration of plasma appears to mimic the cognitive benefits of physical exercise, mitigating postoperative cognitive disturbances in non-exercised animals.

Systemic plasma administration mimics the protective effects of exercise against postoperative hippocampal synaptic deficits

To assess the influence of physical activity and the infusion of exercise-conditioned plasma on neuropathological alterations within the HPC post-anesthesia and surgery, the expression of synaptic proteins and the ultrastructure of synapses were analyzed using IF, WB and TEM. As depicted in IF staining (Fig. 2A-D) and WB (Fig. 2K-M), anesthesia and surgery led to a decline in hippocampal levels of SYP and PSD-95 in the Sur group (*P* values < 0.001 vs. Con) rather than the Ex + Sur (*P* values < 0.001 vs. Sur) and ExP + Sur groups (*P* values < 0.001 vs. Sur), which was consistent with behavioral changes. Further, TEM image analysis (Fig. 2E-F) corroborated these findings, revealing similar patterns in hippocampal synapse density alterations across the groups. Synaptic plasticity, the adaptive capacity of neuronal networks that is fundamental to learning and memory, is known to be compromised under POCD conditions [6, 15]. To elucidate the effects of exercise and exercise plasma on synaptic plasticity within the HPC following anesthesia and surgery, we conducted IF (Fig. 2G-J) and WB (Fig. 2N-P) to evaluate the phosphorylation state and activation of CREB, a pivotal mediator of synaptic plasticity [64], and the expression levels of c-fos, product of the immediate early gene *Fos* implicated in modulating neuronal excitability and synaptic potency [65]. Comparative analysis revealed that the Sur group exhibited a marked reduction in p-CREB and c-fos expression within the HPC relative to the Con group (*P* values < 0.001). The decrease was notably prevented to a similar extent in the Ex + Sur (*P* values < 0.001 vs. Sur) and ExP + Sur groups (*P* values < 0.05 vs. Sur). Altogether, these data indicate that physical exercise confers neuroprotective effects against surgery-induced synaptic deficits, an effect that can be recapitulated through the systemic delivery of plasma derived from exercised mice.

Systemic plasma administration mimics the inhibitory effects of exercise on postoperative hippocampal neuroinflammation

Neuroinflammation, a crucial mechanism in senescence-related neuroinflammatory and neurodegenerative diseases, involves the activation and proinflammatory/potentially detrimental phenotypes of microglia and astrocytes [14, 28]. To assess the impact of exercise and exercise-conditioned plasma on anesthesia/surgery-induced neuroinflammation, we measured the expression and localization of canonical microglia marker IBA1, proinflammatory microglial marker iNOS, well-established astrocyte marker GFAP, and reactive astrocyte marker C3 within the HPC [10, 13]. IF combined with WB analyses revealed elevated hippocampal expression of IBA1, iNOS, GFAP, and C3 in the Sur group compared to the Con group (Fig. 3A-D, F-H, I-L, N-P; all *P* values < 0.05 vs. Con). Colocalization analyses showed increased Pearson correlation coefficients for iNOS with IBA1 (Fig. 3E; $P < 0.001$ vs. Con) and C3 with GFAP (Fig. 3M; $P < 0.001$ vs. Con) in the Sur group, indicating anesthesia/surgery-induced activation of pro-inflammatory microglia and reactive astrocytes. In contrast, these glial responses within the HPC were nearly abolished in the Ex + Sur group (all *P* values < 0.05 vs. Sur). While the absolute R values suggest weak to moderate correlations, the consistent and statistically significant differences between groups provide meaningful insights into relative changes in protein colocalization under various conditions. Furthermore, these intergroup differences in Pearson correlation R values align with and are supported by the trends observed in the analysis results of the Manders coefficient (Fig.S2), another robust indicator for fluorescence colocalization analysis. Similarly, the ExP + Sur group also exhibited reduced proinflammatory microglia and reactive astrocytes (all *P* values < 0.05 vs. Sur). These findings suggest that the inhibitory effects of exercise on anesthesia/surgery-induced hippocampal neuroinflammation can be mimicked via systemic plasma infusion in sedentary mice.

Systemic plasma administration mimics the recuperative benefits of exercise on the dysregulation of hippocampal BDNF/TrkB signaling following surgery

BDNF is a pivotal regulatory molecule for synaptic plasticity and cognitive function [5, 16]. Additionally, BDNF/ BDNF receptor TrkB signaling, the core mechanism mediating the exercise-triggered cognitive benefits [30], is established to be impaired in POCD [5, 17]. In this study, we explored the effects of exercise and

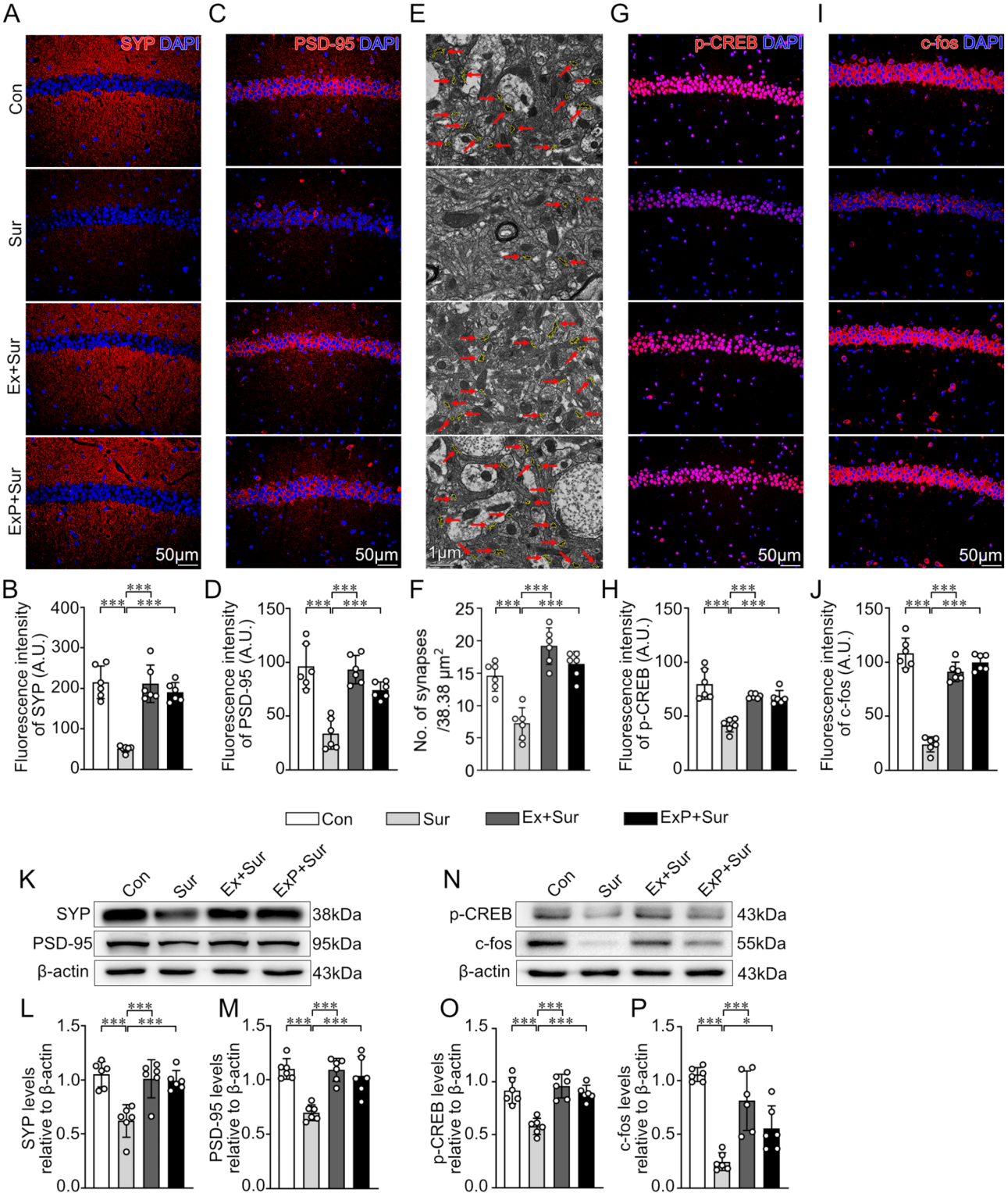

Fig. 2 Exercise-conditioned plasma mimicked the protective effects of exercise on postoperative hippocampal synaptic pathology. (**A**-**D**, **G**-**J**) Representative images of the IF staining to evaluate the expressions of synaptophysin (SYP) (**A**), PSD-95 (**C**), p-CREB (**G**) and c-fos (**I**) in the hippocampal CA1 region and the related statistical analyses (**B**, **D**, **H**, **J**). Scale bars: 50 μm. (**E**-**F**) Representative TEM images of the hippocampal CA1 region with the synapses outlined in yellow and denoted by red arrows (**E**) and the statistical analyses of synapse density (**F**). Scale bars: 1 μm. (**K**-**P**) Representative Western blots of hippocampal SYP, PSD-95 (**K**), p-CREB and c-fos (**N**) and the related statistical analyses (**L**-**M**, **O**-**P**). Data are expressed as mean ± SD; $n = 6$ per group; * $P < 0.05$, ** $P < 0.01$, *** $P < 0.001$

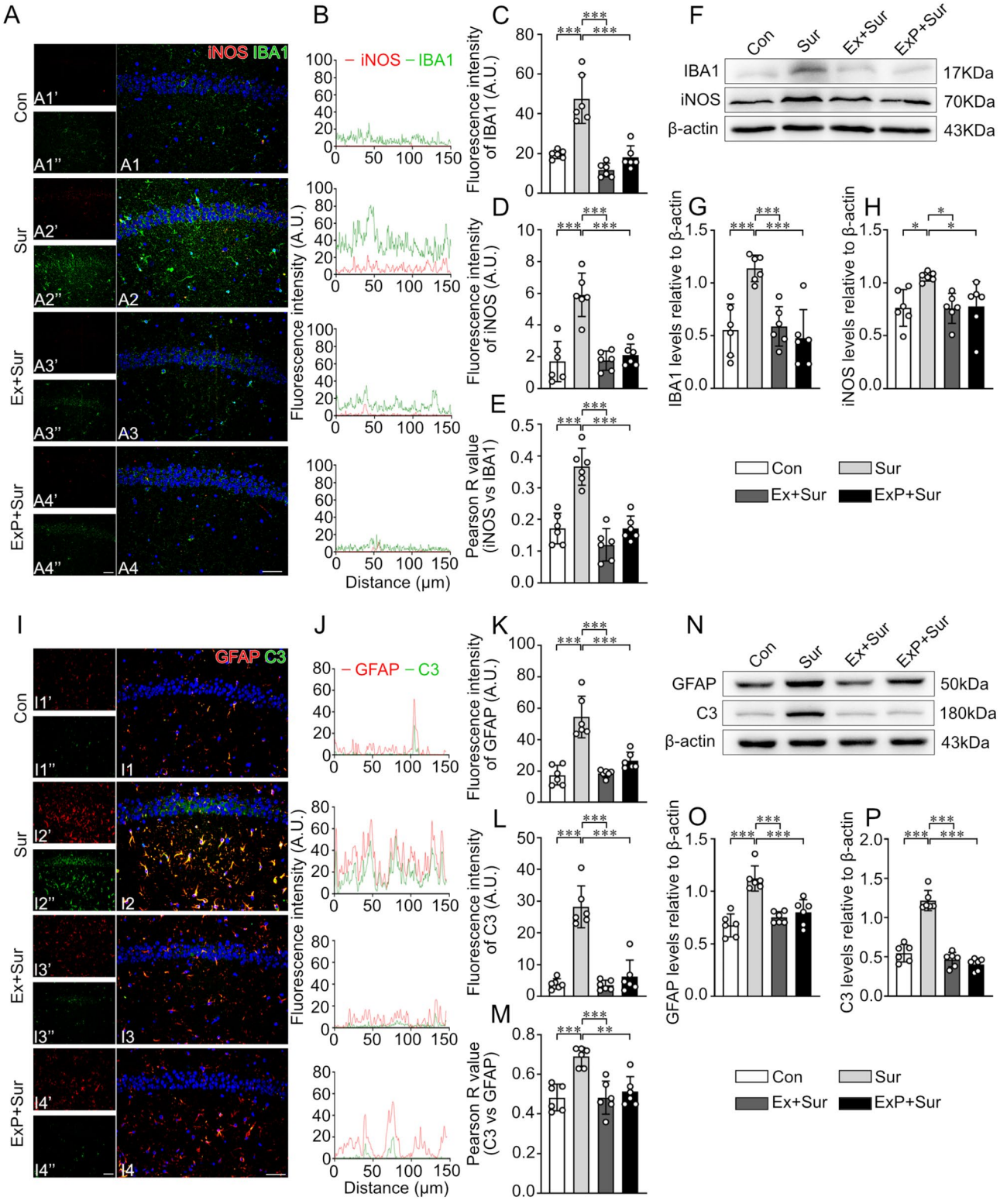

Fig. 3 Exercise-conditioned plasma mimicked the inhibitory effects of exercise on postoperative hippocampal neuroinflammation. (**A**-**B**, **I**-**J**) Representative images of the IF staining to evaluate the colocalization of iNOS with IBA1 (**A**), and C3 with GFAP (**I**) in the hippocampal CA1 region, and the related lineplots of fluorescence intensity (**B**, **J**). Scale bars: 50 μm. (**C**-**D**, **K**-**L**) Statistical analyses of the fluorescence intensity of IBA1 (**C**), iNOS (**D**), GFAP (**K**) and C3 (**L**) in the hippocampal CA1 region. (**E**, **M**) Statistical analyses of the Pearson R value for colocalization of iNOS with IBA1 (**E**), and C3 with GFAP (**M**) in the hippocampal CA1 region. (**F**-**H**, **N**-**P**) Representative Western blots of hippocampal iNOS, IBA1 (**F**), C3 and GFAP (**N**), and the related statistical analyses (**G**-**H**, **O**-**P**). Data are expressed as mean ± SD; $n = 6$ per group; * $P < 0.05$, ** $P < 0.01$, *** $P < 0.001$

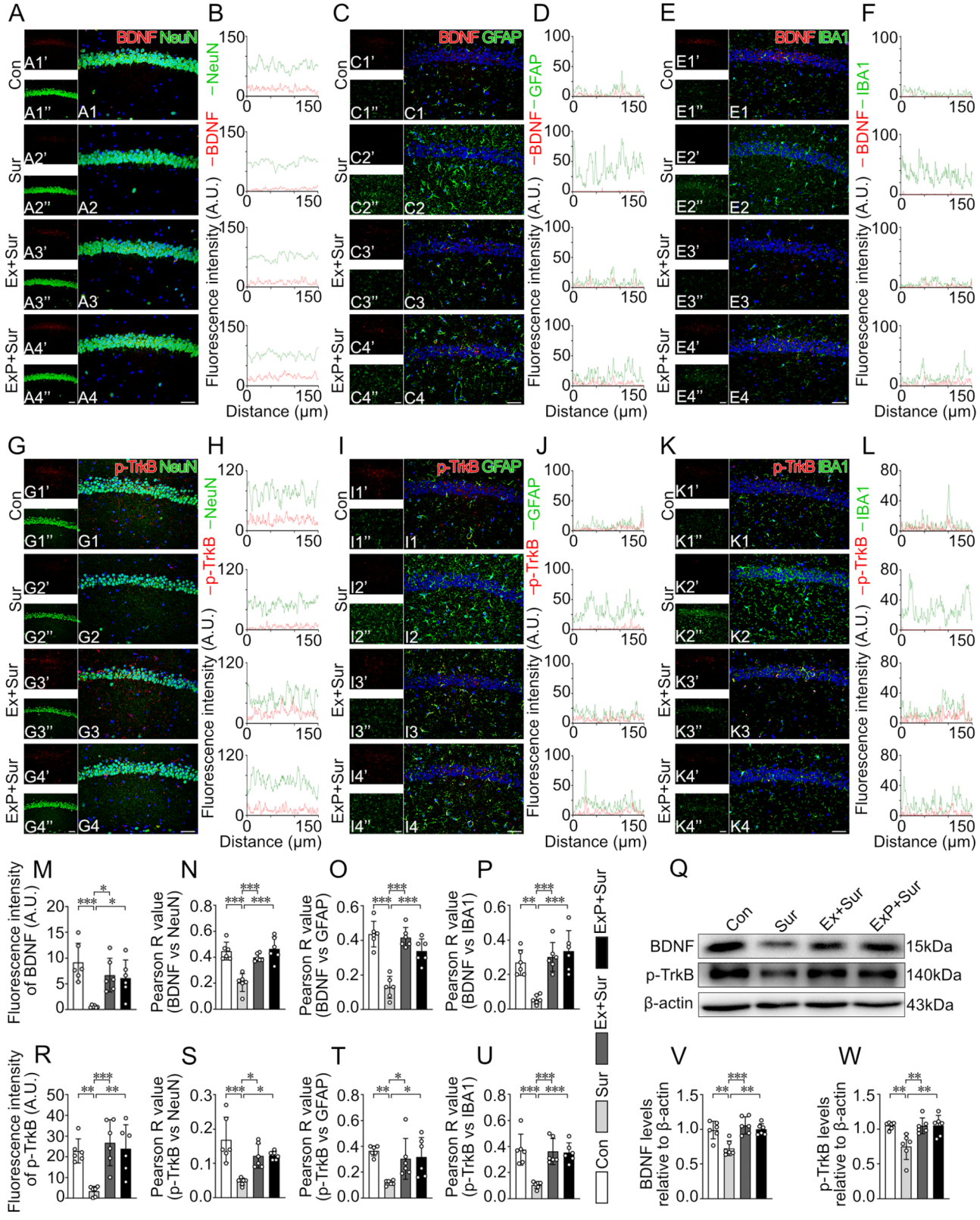

Fig. 4 (See legend on next page.)

(See figure on previous page.)

Fig. 4 Exercise-conditioned plasma mimicked the restoration of postoperative hippocampal BDNF/TrkB signaling by exercise. (**A**-**L**) Representative images of the IF staining to evaluate the colocalization of BDNF with NeuN (**A**), BDNF with GFAP (**C**), BDNF with IBA1 (**E**), p-TrkB (Tyr816) with NeuN (**G**), p-TrkB (Tyr816) with GFAP (**I**) and p-TrkB (Tyr816) with IBA1 (**K**) in the hippocampal CA1 region, and the related lineplots of fluorescence intensity (**B**, **D**, **F**, **H**, **J**, **L**). Scale bars: 50 μm. (**M**, **R**) Statistical analyses of the total fluorescence intensity of BDNF (**M**) and p-TrkB (Tyr816) (**R**) in the hippocampal CA1 region. (**N**-**P**, **S**-**U**) Statistical analyses of the Pearson R value for the colocalization of BDNF with NeuN (**N**), BDNF with GFAP (**O**), BDNF with IBA1 (**P**), p-TrkB (Tyr816) with NeuN (**S**), p-TrkB (Tyr816) with GFAP (**T**), and p-TrkB (Tyr816) with IBA1 (**U**) in the hippocampal CA1 region. (**Q**, **V**-**W**) Representative Western blots of hippocampal BDNF and p-TrkB (Tyr816) (**Q**) and the related statistical analyses (**V**-**W**). Data are expressed as mean ± SD; $n = 6$ per group; * $P < 0.05$, ** $P < 0.01$, *** $P < 0.001$

exercise-conditioned plasma on hippocampal BDNF/TrkB signaling as well as the distribution and potential targets of BDNF under conditions of anesthesia/surgery. As revealed by IF and WB analyses, the Sur group showed marked downregulation in the hippocampal levels of BDNF (Fig. 4A-F, M,Q, V) and activated TrkB (phosphorylated TrkB, p-TrkB (Tyr816)) (Fig. 4G-L, R,Q, W) when compared to the Con group (all *P* values < 0.01). Furthermore, the diminished Pearson correlation coefficients and Manders coefficients for the colocalization of BDNF with NeuN (a canonical neuron marker), GFAP and IBA1 in the Sur group (Fig. 4N-P, Fig. S3A-C; all *P* values < 0.05) suggested surgery-induced reduction in BDNF distribution in neurons, which are the primary source of cerebral BDNF, as well as in astrocytes and microglia, which can also contribute to BDNF production upon stimulation [16, 66]. Whereas, the decreased colocalization correlation coefficients of p-TrkB (Tyr816) with neuronal and glial markers (Fig. 4S-U, Fig. S3D-F; all *P* values < 0.05) indicated a postoperative decline in BDNF responsiveness by hippocampal neurons and potentially by glial cells. In contrast, the BDNF distribution in these cellular populations and the neuronal and glial colocalization with activated TrkB in the HPC were nearly restored in the Ex + Sur group (all *P* values < 0.05 vs. Sur). Similar recovery in hippocampal BDNF distribution and TrkB activation was detected in the ExP + Sur group (all *P* values < 0.05 vs. Sur). These data suggest that exercise mitigates the adverse effects of anesthesia/surgery on BDNF/TrkB signaling, an effect which could be mimicked by systemic infusion of plasma to sedentary mice.

Exercise-conditioned plasma rescues POCD via BDNF/TrkB signaling

To further investigate whether regulation of BDNF signaling is a potential mechanism underlying the therapeutic benefits of exercise-conditioned plasma under conditions of POCD, TrkB was pharmacologically blocked in the ANA12 + ExP + Sur group immediately prior to plasma infusion with ANA-12 (Fig. 5A), which is a blood–brain barrier-permeable, highly selective antagonist against TrkB [46, 67]. As expected, ANA-12 administration attenuated the increase in hippocampal p-TrkB (Tyr816) levels and TrkB activation in neuron, and potentially in astrocytes and microglia, induced by exercise-conditioned plasma (Fig. 5J-O, V-Z, AE; Fig. S4A-C; all *P* values < 0.05 vs. ExP + Sur). Remarkably, the inhibition of TrkB with ANA-12 also suppressed the increase in BDNF distribution in neurons, astrocytes, and microglia within the HPC following exercise plasma administration (Fig. 5P-U, Z-AD, AF; Fig. S4D-F; all *P* values < 0.05 vs. ExP + Sur), which implies the disturbed autocrine and paracrine effects of hippocampal BDNF. Consistently, mice in the ANA12 + ExP + Sur group exhibited significantly reduced exploration in the central zone of OF arena and exaggerated anxiety-like behavior (Fig. 5B, F; $P < 0.001$ vs. ExP + Sur), impaired bias towards the displaced and novel objects in NLR and NOR tasks (Fig. 5C-D, G-H; both *P* values < 0.05 vs. ExP + Sur), and vanished spontaneous alternation in Y maze task (Fig. 5E, I; $P < 0.05$ vs. ExP + Sur), which suggests that TrkB antagonism with ANA-12 abrogated the preventive effects of exercise-conditioned plasma on postoperative decline in HPC-dependent learning and memories. Moreover, inhibiting BDNF/TrkB signaling with ANA-12 hindered the restoration of synaptic protein expression (Fig. 6A-D, K-M; all *P* values < 0.05 vs. ExP + Sur), synapse density and synaptogenesis (Fig. 6E-F; $P < 0.05$ vs. ExP + Sur), and synaptic plasticity regulators (Fig. 6G-J, K,R-S; all *P* values < 0.001 vs. ExP + Sur) in the HPC, triggered by exercise-conditioned plasma. Additionally, the pharmacological antagonism of BDNF/TrkB signaling with ANA-12 nullified the protective effects of exercise plasma against postoperative astrogliosis, microgliosis, and activation of potentially detrimental astrocytes and proinflammatory microglia in the HPC (Fig. 6N-Q, T-AD; Fig. S4G-H; all *P* values < 0.05 vs. ExP + Sur). Similar effects were observed in the ANA12 + Ex + Sur group, where regular exercise training benefits were also negated (Fig. S5-S6; all *P* values < 0.05 vs. Ex + Sur). The consistent results between the ANA12 + ExP + Sur and ANA12 + Ex + Sur groups further corroborate the specificity of ANA-12 in targeting TrkB and underscore the crucial role of BDNF/TrkB signaling in mediating the cognitive preservation effects of both exercise-conditioned plasma and regular exercise. Collectively, these findings suggest that exercise-conditioned plasma rescues anesthesia/surgery-induced cognitive disorder and the corresponding hippocampal synaptic deficits and neuroinflammation, at least partly via BDNF/TrkB signaling.

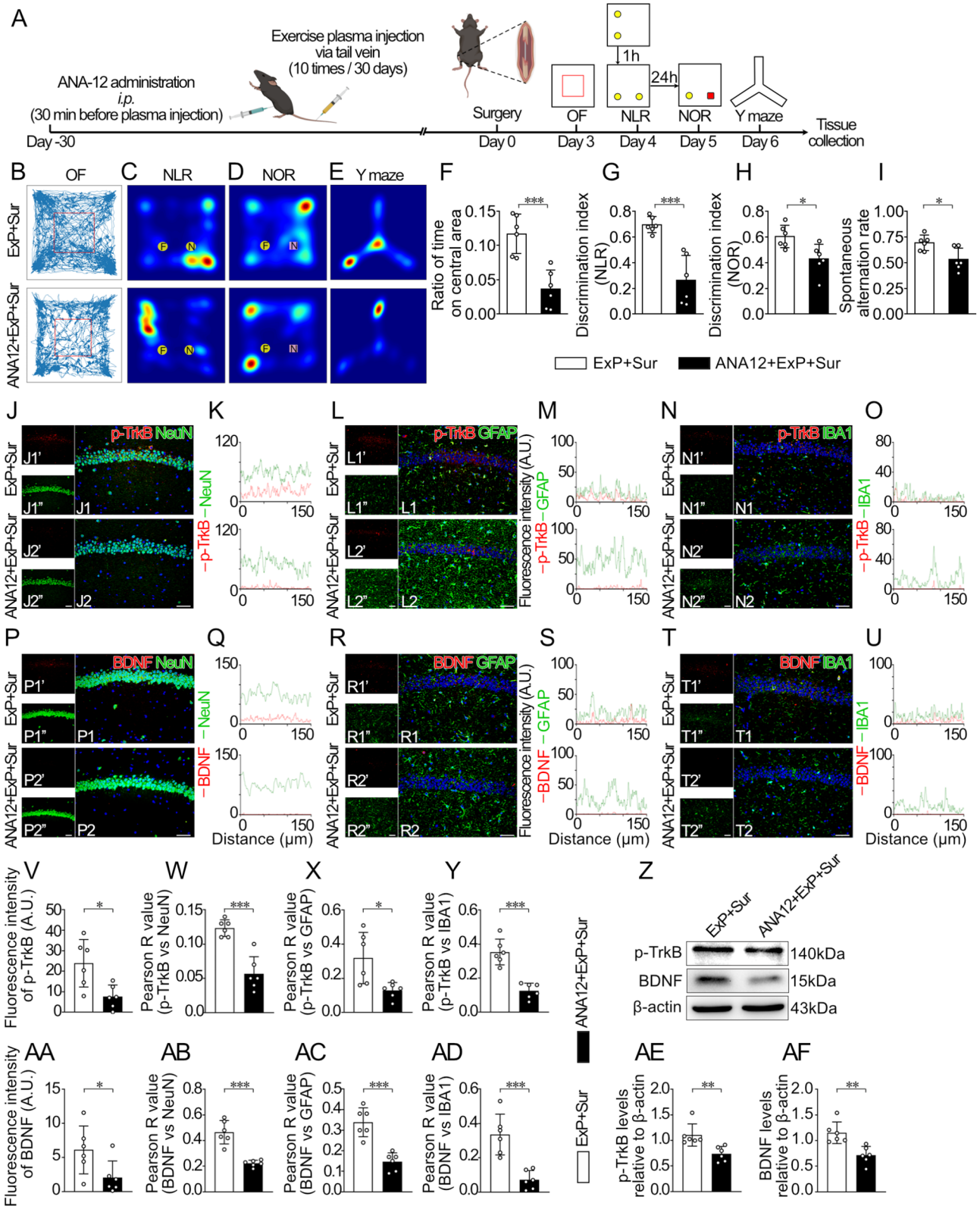

Fig. 5 (See legend on next page.)

(See figure on previous page.)

Fig. 5 ANA-12 blocks hippocampal BDNF/TrkB signaling, attenuating cognitive recovery by exercise plasma. (**A**) Schematic illustration of the experimental design of ANA-12 administration. (**B**, **F**) Representative locus diagrams and the statistical analyses of the OF tests. (**C**-**E**, **G**-**I**) Representative trajectory heat maps and the related statistical analyses of the NLR (**C**, **G**), NOR (**D**, **H**) and Y maze tests (**E**, **I**). (**J**-**U**) Representative images of the IF staining to evaluate the colocalization of p-TrkB (Tyr816) with NeuN (**J**), p-TrkB (Tyr816) with GFAP (**L**), p-TrkB (Tyr816) with IBA1 (**N**), BDNF with NeuN (**P**), BDNF with GFAP (**R**) and BDNF with IBA1 (**T**) in the hippocampal CA1 region, and the related lineplots of fluorescence intensity (**K**, **M**, **O**, **Q**, **S**, **U**). Scale bars: 50 μm. (**V**, **AA**) Statistical analyses of the total fluorescence intensity of p-TrkB (Tyr816) (**V**) and BDNF (**AA**) in the hippocampal CA1 region. (**W**-**Y**, **AB**-**AD**) Statistical analyses of the Pearson R value for the colocalization of p-TrkB (Tyr816) with NeuN (**W**), p-TrkB (Tyr816) with GFAP (**X**), p-TrkB (Tyr816) with IBA1 (**Y**), BDNF with NeuN (**AB**), BDNF with GFAP (**AC**), and BDNF with IBA1 (**AD**) in the hippocampal CA1 region. (**Z**, **AE**-**AF**) Representative Western blots of hippocampal p-TrkB (Tyr816) and BDNF (**Z**) and the related statistical analyses (**AE**-**AF**). Data are expressed as mean ± SD; $n = 6$ per group; * $P < 0.05$, ** $P < 0.01$, *** $P < 0.001$

Systemic plasma administration mimics the protective benefits of exercise on postoperative hippocampal cholinergic dysfunction

Cholinergic networks play a crucial role in the complex regulation of neural oscillation and synaptic plasticity, which are essential for cognition [38]. Enhancing cholinergic signaling in non-human primates and mice with Prion neurodegeneration or sepsis-induced encephalopathy has been shown to improve various cognitive domains [43, 47, 50]. The cholinergic circuits in the MS-HPC are susceptible to aging, neurodegenerative diseases, and POCD [12, 53, 54]. Notably, sustained moderate physical exercise training or exposure to youthful blood with rejuvenating properties can ameliorate senescence and AD-related cholinergic defects in the HPC [53, 54]. To evaluate the effects of exercise and exercise-conditioned plasma on the hippocampal cholinergic circuit in the context of POCD, we analyzed hippocampal cholinergic innervation and its neuronal sources in the basal forebrain. Using IHC and WB analyses, we found a significant decrease in the integrated density of CHAT in hippocampal cholinergic afferent fibers and MS cholinergic neurons in the surgery group (Fig. 7A-D, L-M; all P values < 0.01 vs. Con). The deficits in hippocampal cholinergic innervation and degeneration of MS cholinergic neurons induced by anesthesia/surgery were significantly mitigated in the Ex + Sur (all P values < 0.001 vs. Sur) and ExP + Sur groups (all P values < 0.05 vs. Sur). To assess hippocampal responsiveness to cholinergic input, we examined the expression and localization of CHRM1, a key hippocampal cholinergic receptor involved in cognitive modulation [38, 43, 46]. We observed reduced total levels of hippocampal CHRM1 and its diminished colocalization with neuron and astrocyte markers in the Sur group (Fig. 7E-K, L,N; Fig. S7; all P values < 0.01 vs. Con). Conversely, the downregulated total, neuronal, and astroglial expressions of CHRM1 following surgery were restored by exercise training (Ex + Sur: all P values < 0.01 vs. Sur) or systemic infusion of exercise-conditioned plasma from exercised mice (ExP + Sur: all P values < 0.05 vs. Sur). To evaluate the activity of the hippocampal cholinergic system, we measured ACh levels. Consistent with changes in cognition and the structure of the hippocampal cholinergic circuit, the anesthesia/surgery-induced decline in ACh release (Fig. 7O; Sur: $P < 0.001$ vs. Con) was normalized by treatments with exercise (Ex + Sur: $P < 0.001$ vs. Sur) and exercise-conditioned plasma (ExP + Sur: $P < 0.01$ vs. Sur). These findings collectively indicate that exercise-conditioned plasma reproduces the protective effects of exercise on postoperative hippocampal cholinergic dysfunction.

Exercise-conditioned plasma rescues POCD by activating the hippocampal cholinergic circuit

To explore whether activation of the basal forebrain-hippocampal cholinergic circuit is a potential mediator underpinning the beneficial effects of exercise-conditioned plasma on POCD, CHRM1 was pharmacologically blocked with THP in the THP + ExP + Sur group immediately prior to plasma administration (Fig. 8A). THP is a blood-brain barrier-permeable, highly selective antagonist against CHRM1, without risks of impairing cognitive function itself [68]. CHRM1 antagonism with THP significantly impaired the exercise-conditioned plasma-boosted recovery of exploratory activity and anxiety-like behavior (OF; Fig. 8B, F), preference for novel stimuli and retention of discriminative memory (NLR and NOR; Fig. 8C-D, G-H), and spontaneous alternation behavior and spatial working memory (Y maze; Fig. 8E, I) in mice receiving POCD surgery (THP + ExP + Sur: all P values < 0.01 vs. ExP + Sur). Intriguingly, THP administration under conditions of POCD notably abolished the exercise-conditioned plasma-induced reversal of the density of hippocampal $CHAT^+$ cholinergic afferent fibers (Fig. 8J, P,Q, X), CHAT expression in the sources of hippocampal cholinergic input (MS; Fig. 8K, R), hippocampal levels and neuronal and astroglial localization of CHRM1 (Fig. 8L-O, S-V, X; Fig. S8A-B), and hippocampal ACh release and cholinergic activation (Fig. 8W) (THP + ExP + Sur: all P values < 0.01 vs. ExP + Sur). Furthermore, blocking hippocampal cholinergic activity using THP hindered the postoperative recovery of hippocampal synapse formation (Fig. 8X-Z, AD-AG), synapse ultrastructure (Fig. 8AA, AH), and synaptic plasticity (Fig. 8X, AB-AC, AI-AL) in response to exercise-conditioned plasma, and impeded the preventive benefits of exercise plasma on surgery-induced gliosis, reactive state of astrocytes, and pro-inflammatory state of microglia (Fig. 9A-E, R-AA; Fig. S8C-D) (THP + ExP + Sur: all P values < 0.05 vs. ExP + Sur). Mechanistically, inhibition of the

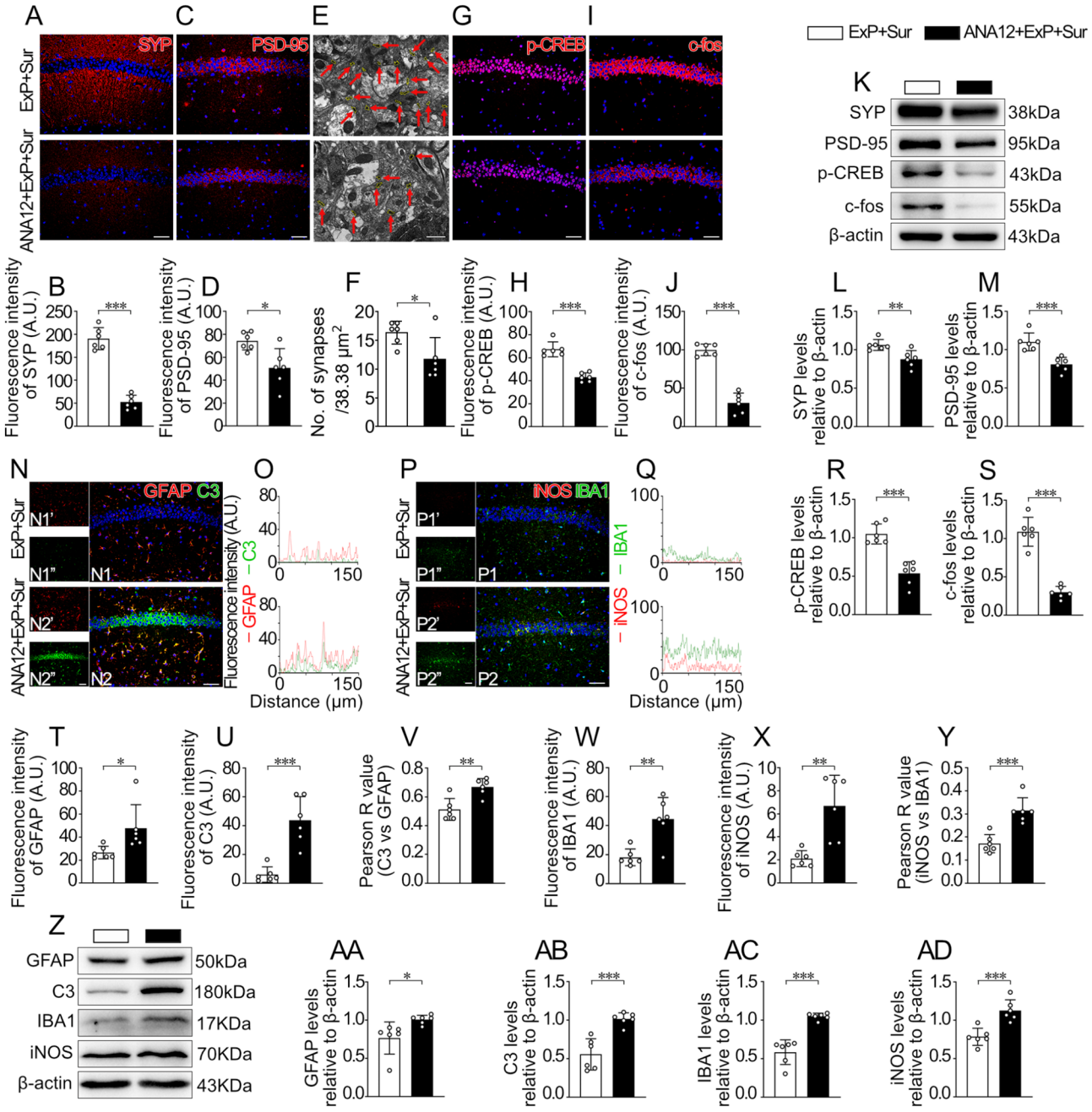

Fig. 6 ANA-12 blocks BDNF/TrkB signaling, reducing synaptic and anti-inflammatory benefits of exercise plasma. (**A**-**D**, **G**-**J**) Representative images of the IF staining to evaluate the expressions of SYP (**A**), PSD-95 (**C**), p-CREB (**G**) and c-fos (**I**) in the hippocampal CA1 region and the related statistical analyses (**B**-**D**, **H**-**J**). Scale bars: 50 μm. (**E**-**F**) Representative TEM images of the the hippocampal CA1 region with the synapses outlined in yellow and denoted by red arrows (**E**) and the statistical analyses of synapse density (**F**). Scale bars: 1 μm. (**K**-**M**, **R**-**S**, **Z**-**AD**) Representative Western blots of hippocampal SYP, PSD-95, p-CREB, c-fos (**K**), GFAP, C3, iNOS and IBA1 (**Z**), and the related statistical analyses (**L**-**M**, **R**-**S**, **AA**-**AD**). (**N**-**Q**) Representative images of the IF staining to evaluate the colocalization of C3 with GFAP (**N**), and iNOS with IBA1 (**P**) in the hippocampal CA1 region, and the related lineplots of fluorescence intensity (**O**, **Q**). Scale bars: 50 μm. (**T**-**U**, **W**-**X**) Statistical analyses of the fluorescence intensity of GFAP (**T**), C3 (**U**), IBA1 (**W**) and iNOS (**X**) in the hippocampal CA1 region. (**V**, **Y**) Statistical analyses of the Pearson R value for colocalization of C3 with GFAP (**V**), and iNOS with IBA1 (**Y**) in the hippocampal CA1 region. Data are expressed as mean ± SD; $n = 6$ per group; * $P < 0.05$, ** $P < 0.01$, *** $P < 0.001$

hippocampal cholinergic system by THP attenuated the exercise-conditioned plasma-induced increase in total hippocampal BDNF levels as well as BDNF distribution in neurons, astrocytes, and microglia, and consequently the neuronal TrkB activation and potential BDNF-related effects on glial cells (Fig. 9E-Q, AB-AK; Fig. S8E-J; THP + ExP + Sur: all P values < 0.05 vs. ExP + Sur). Similar effects were observed in the THP + Ex + Sur control

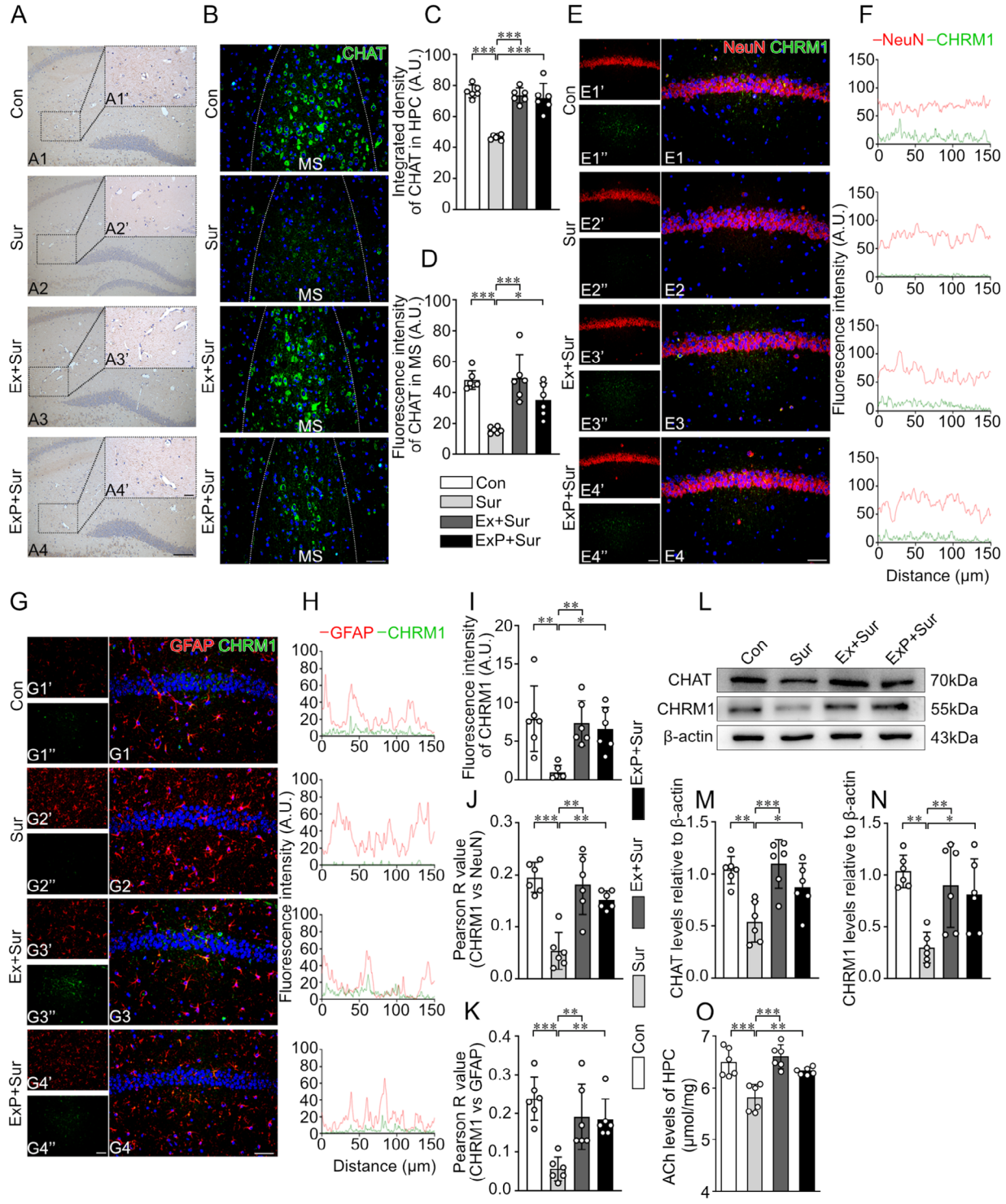

Fig. 7 Exercise-conditioned plasma mitigated postoperative dysfunction of MS-hippocampal cholinergic circuit. (**A**, **C**) Representative images of the IHC staining to evaluate the expressions of CHAT (**A**) in the hippocampal CA3 region and the related statistical analyses (**C**). Scale bars (A1-A4): 200 μm; (A1'-A4'): 50 μm. (**B**, **D**) Representative images of the IF staining to evaluate the expressions of CHAT (**B**) in the MS and the related statistical analyses (**D**). Scale bars: 50 μm. (**E**-**H**) Representative images of the IF staining to evaluate the colocalization of CHRM1 with NeuN (**E**), and CHRM1 with GFAP (**G**) in the hippocampal CA1 region, and the related lineplots of fluorescence intensity (**F**, **H**). Scale bars: 50 μm. (**I**) Statistical analyses of the total fluorescence intensity of CHRM1 in the hippocampal CA1 region. (**J**, **K**) Statistical analyses of the Pearson R value for colocalization of CHRM1 with NeuN (**J**), and CHRM1 with GFAP (**K**) in the hippocampal CA1 region. (**L**-**N**) Representative Western blots of hippocampal CHAT and CHRM1 (**L**), and the related statistical analyses (**M**-**N**). (**O**) Statistical analyses of the levels of hippocampal ACh. Data are expressed as mean ± SD; $n = 6$ per group; * $P < 0.05$, ** $P < 0.01$, *** $P < 0.001$

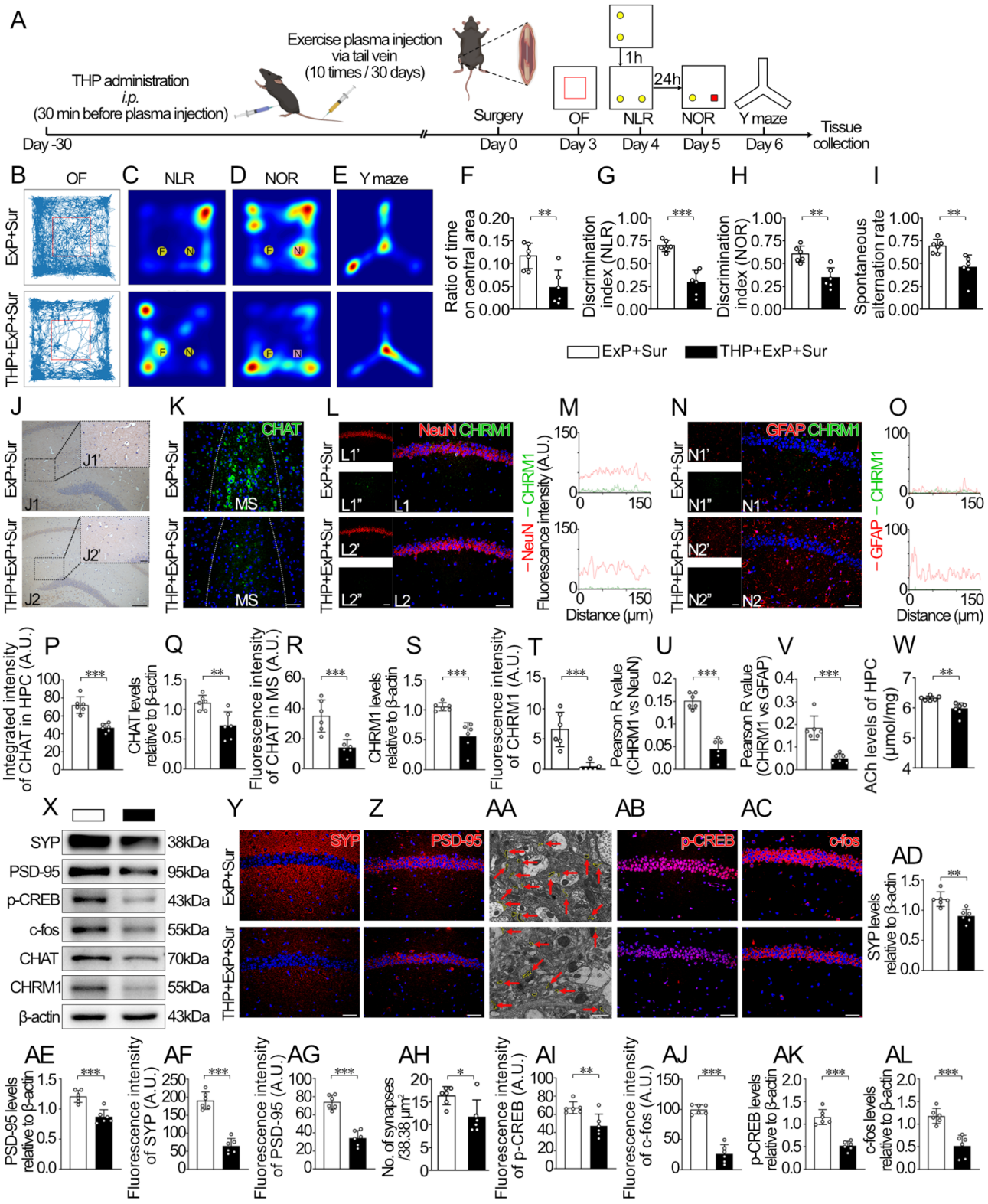

Fig. 8 (See legend on next page.)

(See figure on previous page.)

Fig. 8 THP inhibits MS-hippocampal cholinergic activity, reducing cognitive and synaptic recovery by exercise plasma. (**A**) Schematic illustration of the experimental design of THP administration. (**B**, **F**) Representative locus diagrams and the statistical analyses of the OF tests. (**C**-**E**, **G**-**I**) Representative trajectory heat maps and the related statistical analyses of the NLR (**C**, **G**), NOR (**D**, **H**) and Y maze tests (**E**, **I**). (**J**, **P**) Representative images of the IHC staining to evaluate the expressions of CHAT (**J**) in the hippocampal CA3 region and the related statistical analyses (**P**). Scale bars (J1-J2): 200 μm; (J1'-J2'): 50 μm. (**K**, **R**) Representative images of the IF staining to evaluate the expressions of CHAT (**K**) in the MS and the related statistical analyses (**R**). Scale bars: 50 μm. (**L**-**O**) Representative images of the IF staining to evaluate the colocalization of CHRM1 with NeuN (**L**), and CHRM1 with GFAP (**N**) in the hippocampal CA1 region, and the related lineplots of fluorescence intensity (**M**, **O**). Scale bars: 50 μm. (**T**) Statistical analyses of the total fluorescence intensity of CHRM1 in the hippocampal CA1 region. (**U**, **V**) Statistical analyses of the Pearson R value for colocalization of CHRM1 with NeuN (**U**), and CHRM1 with GFAP (**V**) in the hippocampal CA1 region. (**W**) Statistical analyses of the levels of hippocampal ACh. (**Q**, **S**, **X**, **AD**-**AE**, **AK**-**AL**) Representative Western blots of hippocampal CHAT, CHRM1, SYP, PSD-95, p-CREB and c-fos (**X**), and the related statistical analyses (**Q**, **S**, **AD**-**AE**, **AK**-**AL**). (**Y**-**Z**, **AB**-**AC**, **AF**-**AG**, **AI**-**AJ**) Representative images of the IF staining to evaluate the expressions of SYP (**Y**), PSD-95 (**Z**), p-CREB (**AB**) and c-fos (**AC**) in the hippocampal CA1 region and the related statistical analyses (**AF**-**AG**, **AI**-**AJ**). Scale bars: 50 μm. (**AA**, **AH**) Representative TEM images of the hippocampal CA1 region with the synapses outlined in yellow and denoted by red arrows (**AA**) and the statistical analyses of synapse density (**AH**). Scale bars: 1 μm. Data are expressed as mean ± SD; $n = 6$ per group; * $P < 0.05$, ** $P < 0.01$, *** $P < 0.001$

group, where regular exercise training benefits were also negated (Fig. S9-S10; all P values < 0.05 vs. Ex + Sur). The consistency of results between the THP + ExP + Sur and THP + Ex + Sur groups further supports the specificity of THP in targeting CHRM1 activity and the role of CHRM1 in mediating exercise/ exercise-conditioned plasma-related cognitive benefits.

Given the exercise-conditioned plasma-induced hippocampal CHRM1 expression parallel to cognitive recovery, to investigate whether CHRM1-mediated cholinergic activity is a potential mechanism underlying the therapeutic effects of exercise plasma on POCD, in vivo knockdown of *Chrm1* expression was performed in the shRNA + ExP + Sur group by stereotaxic injection of AAV2/5-U6-*Chrm1* shRNA-CMV-EGFP-WPRE into bilateral HPC (Fig. 10A). Expectedly, injection of the AAV vector expressing *Chrm1* shRNA silenced the CHRM1 expression in the infected HPC and abrogated the upregulation of neuronal and astrocyte CHRM1 in response to exercise-conditioned plasma (Fig. 10J-N, P-S, AC; Fig. S11A-B; shRNA + ExP + Sur: all P values < 0.01 vs. NC + ExP + Sur). Notably, in vivo knockdown of hippocampal *Chrm1* attenuated the exercise-conditioned plasma-induced restoration of $CHAT^+$ cholinergic innervation and ACh release in hippocampal under conditions of POCD (Fig. 10O, T,W, AC, AK; shRNA + ExP + Sur: all P values < 0.05 vs. NC + ExP + Sur). Analogous to pharmacological antagonism, silencing of hippocampal *Chrm1* with the AAV vector significantly restrained the improvement in learning and exploratory behavior and anxiety-like behavior (OF), spatial reference memory and retention-based discrimination (NLR and NOR), and spatial working memory-dependent spontaneous alternation (Y maze) triggered by exercise-conditioned plasma in mice subjected to POCD surgery (Fig. 10B-I; shRNA + ExP + Sur: all P values < 0.05 vs. NC + ExP + Sur). Moreover, *Chrm1* silencing in the HPC led to failures in the exercise-conditioned plasma-responsive reversal of hippocampal synaptogenesis (Fig. 10U-V, X-Z, AC-AF), synaptic plasticity (Fig. 10AA-AC, AG-AJ), and neuroinflammation-related proliferation and activation of reactive astrocytes and proinflammatory microglia following surgery (Fig. 11A-E, R-AA; Fig. S11C-D) (shRNA + ExP + Sur: all P values < 0.05 vs. NC + ExP + Sur). Mechanistically, *Chrm1* knockdown suppressed the exercise plasma-promoted postoperative recovery of hippocampal BDNF distribution in neurons, astrocytes, and microglia, and accordingly BDNF-stimulated neuronal TrkB activation and potential effects on glial cells (Fig. 11E-Q, AB-AL; Fig. S11E-I; shRNA + ExP + Sur: the main P values < 0.01 vs. NC + ExP + Sur). Collectively, these data suggest that exercise-conditioned plasma exerts protective effects on POCD at least partly via CHRM1-mediated hippocampal cholinergic activity.

Discussion

Cumulatively, our data confirm that exercise-conditioned plasma mimics the protective effects of exercise on anesthesia/surgery-induced neuroinflammation and impairments in synaptic functions and hippocampal-dependent learning and memory to sedentary aged mice. Mechanistically, we identified CHRM1-dependent hippocampal cholinergic activity-regulated BDNF/TrkB signaling as the mediator of exercise plasma that attenuates postoperative hippocampal neuropathological events and cognitive decline.

POCD is a common complication after anesthesia and surgery, affecting multiple cognitive functions (such as memory and mood), and can last for weeks to years [1–3, 5]. It occurs in 10-54% of surgery patients, especially those aged 65 and older, leading to increased postoperative mortality and decreased quality of life [6–8]. Neuroinflammation is established as the vital mediator in POCD, triggered by anesthesia/surgery-induced systemic inflammation effectors (such as TNFα, IL-1β, and IL-6). These effectors cause abnormal activation of microglia and astrocytes, shifting them to pro-inflammatory and potentially detrimental states, leading to neuronal dysfunction [6, 10–14]. The resulting neuronal dysfunction, marked by impaired synaptic plasticity, affects learning and memory, as synapses are crucial for neuronal communication and circuit dynamics [6, 15]. Common

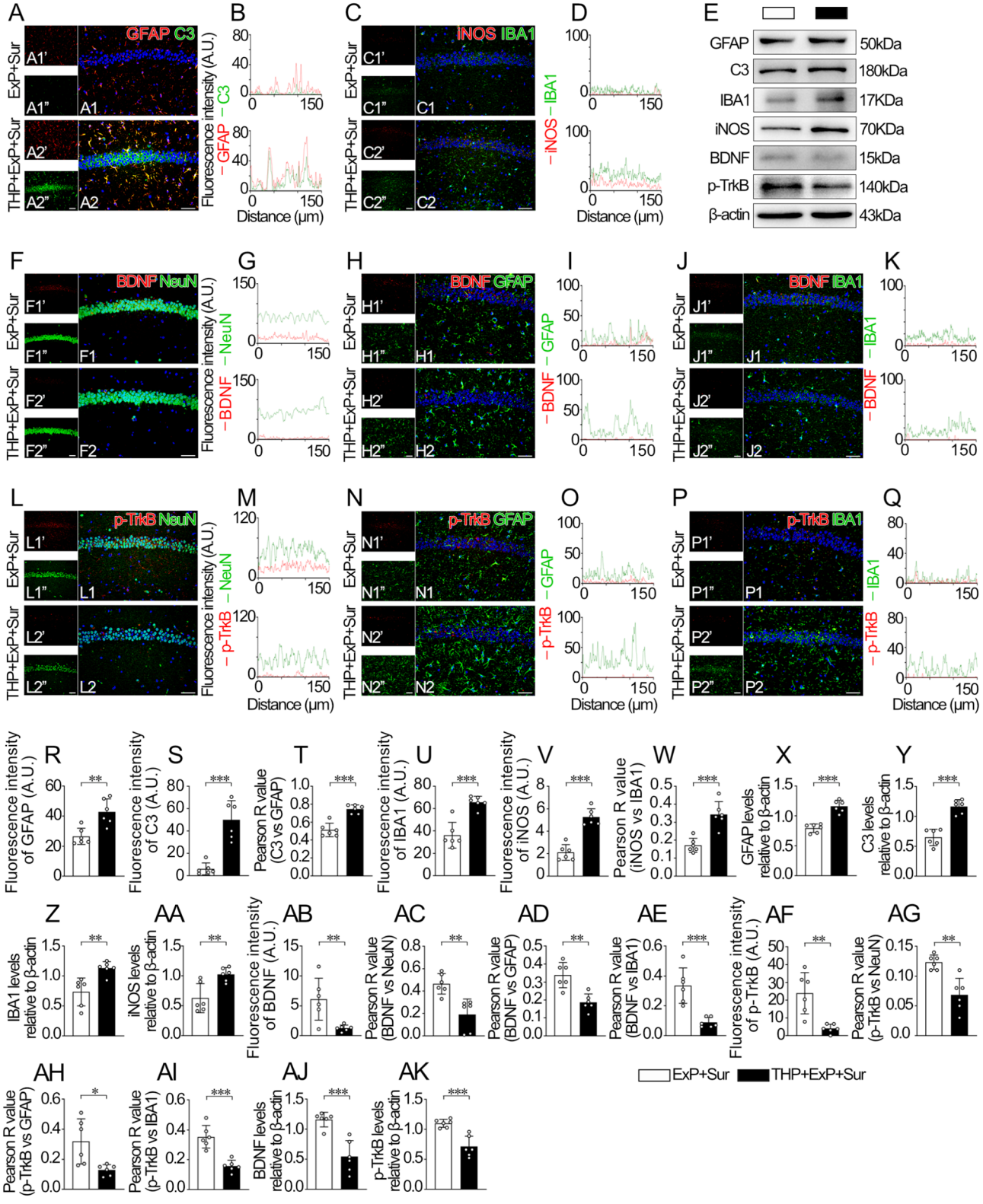

Fig. 9 (See legend on next page.)

(See figure on previous page.)

Fig. 9 THP administration attenuates the exercise-conditioned plasma-induced postoperative recovery from neuroinflammation and BDNF/TrkB dysfunction. (**A**-**D**, **F**-**Q**) Representative images of the IF staining to evaluate the colocalization of C3 with GFAP (**A**), and iNOS with IBA1 (**C**), BDNF with NeuN (**F**), BDNF with GFAP (**H**), BDNF with IBA1 (**J**), p-TrkB (Tyr816) with NeuN (**L**), p-TrkB (Tyr816) with GFAP (**N**) and p-TrkB (Tyr816) with IBA1 (**P**) in the hippocampal CA1 region, and the related lineplots of fluorescence intensity (**B**, **D**, **G**, **I**, **K**, **M**, **O**, **Q**). Scale bars: 50 μm. (**E**, **X**-**AA**, **AJ**-**AK**) Representative Western blots of hippocampal C3, GFAP, iNOS, IBA1, BDNF and p-TrkB (Tyr816) (**E**), and the related statistical analyses (**X**-**AA**, **AJ**-**AK**). (**R**-**S**, **U**-**V**, **AB**, **AF**) Statistical analyses of the total fluorescence intensity of GFAP (**R**), C3 (**S**), IBA1 (**U**), iNOS (**V**), BDNF (**AB**) and p-TrkB (Tyr816) (**AF**) in the hippocampal CA1 region. (**T**, **W**, **AC**-**AE**, **AG**-**AI**) Statistical analyses of the Pearson R value for the colocalization of C3 with GFAP (**T**), iNOS with IBA1 (**W**), BDNF with NeuN (**AC**), BDNF with GFAP (**AD**), BDNF with IBA1 (**AE**), p-TrkB (Tyr816) with NeuN (**AG**), p-TrkB (Tyr816) with GFAP (**AH**), and p-TrkB (Tyr816) with IBA1 (**AI**) in the hippocampal CA1 region. Data are expressed as mean ± SD; $n = 6$ per group; * $P < 0.05$, ** $P < 0.01$, *** $P < 0.001$

rodent models used for POCD studies include carotid artery exposure surgery [27], exploratory laparotomy [18], and tibial fracture surgery under anesthesia [3, 6, 69]. In this study, we performed the canonical tibia fracture surgery under general anesthesia on aging male mice (17 months) to establish the POCD model. This procedure requires only about 15 min per animal, resulting in zero to minimal mortality, without significantly confounding tasks in behavioral paradigms due to adequate locomotor stabilization [3, 69]. To address potential confounding effects of surgery on motor performance, we analyzed the average velocity of mice during the OF test (Fig.S1), which showed no significant differences between groups. This suggests that the observed cognitive effects are not due to changes in general locomotor activity. The timeline for behavioral tests (days 3–6 post-surgery) was chosen based on previous studies showing significant cognitive impairment and neuroinflammation in aged mice within 72 h after POCD model surgery [27, 70], persisting for at least 5–7 days [27, 71]. This timeframe allows for the detection of cognitive changes similar to those observed in early stages of clinical POCD. While our model cannot fully replicate the long-term effects seen in humans, where POCD can last for weeks to years [4, 5], it offers valuable insights into the early mechanisms of POCD, which are critical for understanding its onset and progression. We selected this age model to reflect the human elderly population susceptible to POCD, as 17-month-old mice are approximately equivalent to 69-year-old humans in terms of age-related biological processes [72]. Although this model provides significant insights into POCD in aging, we acknowledge that additional research may be necessary to fully elucidate the translational implications of our findings to the diverse elderly human population. Aged mice receiving pure tibial fracture under general anesthesia surgery in the absence of any therapeutic treatment exhibited decreased overall exploratory activity, elevated anxiety-like behavior levels, impaired bias towards novel stimuli and retention of discrimination memory, and negatively affected spatial working memory as shown in behavioral tests (Fig. 1). This is consistent with the decrease in expressions of pre- (SYP) and post-synaptic (PSD-95) markers, density of synaptic ultrastructure, and levels of synaptic plasticity regulators (p-CREB and c-fos; Fig. 2), as well as the increase in the activated $iNOS^+$ pro-inflammatory microglia and $C3^+$ reactive astrocytes within the HPC (Fig. 3). Taken together, the animal model used in this study recapitulated the main functional and pathological features of POCD. Despite numerous attempts in preclinical studies, there are currently no effective clinical preventive or therapeutic strategies.

Regular exercise significantly enhances cognitive performance in patients and animal models with aging conditions and neurodegenerative or cerebrovascular diseases, including AD, PD, frontotemporal degeneration, and vascular dementia [19–21, 23, 24]. It also aids recovery from cognitive impairments associated with treatments like radiotherapy, chemotherapy, and surgery, as shown by preclinical and clinical studies [15, 25–27]. Consistent with previous reports, we observed in this study that 30-day voluntary exercise on running wheels prior to surgery prevented dysfunction in multiple HPC-dependent cognitive functions (Fig. 1) and contemporaneously mitigated compromised synaptogenesis and synaptic plasticity following anesthesia/surgery (Fig. 2). The anti-neuroinflammatory effects of exercise may contribute to cognitive protection. Exercise training modulates the activation states of microglia and astrocytes, shifting them from pro-inflammatory towards neuroprotective and neurotrophic states, thereby improving cognitive function [32, 33]. Our data reveal that exercise training on running wheels resulted in diminished postoperative activation of pro-inflammatory microglia and reactive astrocytes in the HPC, in parallel with cognitive and synaptic recovery (Fig. 3). These findings confirm the therapeutic potential of the exercise paradigms utilized in this study.

Noteworthily, several rigorous studies implicate blood factors in the cognitive benefits of exercise. Plasma from exercise-trained mice improves hippocampal neurogenesis, reduces neuroinflammation, and enhances cognitive functions in sedentary model mice of aging, acute brain inflammation, and AD, with Gpld1, clusterin, and platelet factor 4 recognized as crucial mediators [34–36]. The identification of various exercise-related pro-cognitive blood factors in different studies may be attributable to the complexity of exercise effects, as exercise induces changes in the expression of over 200 secreted protein pairs across multiple tissues and cell types in mice [37].

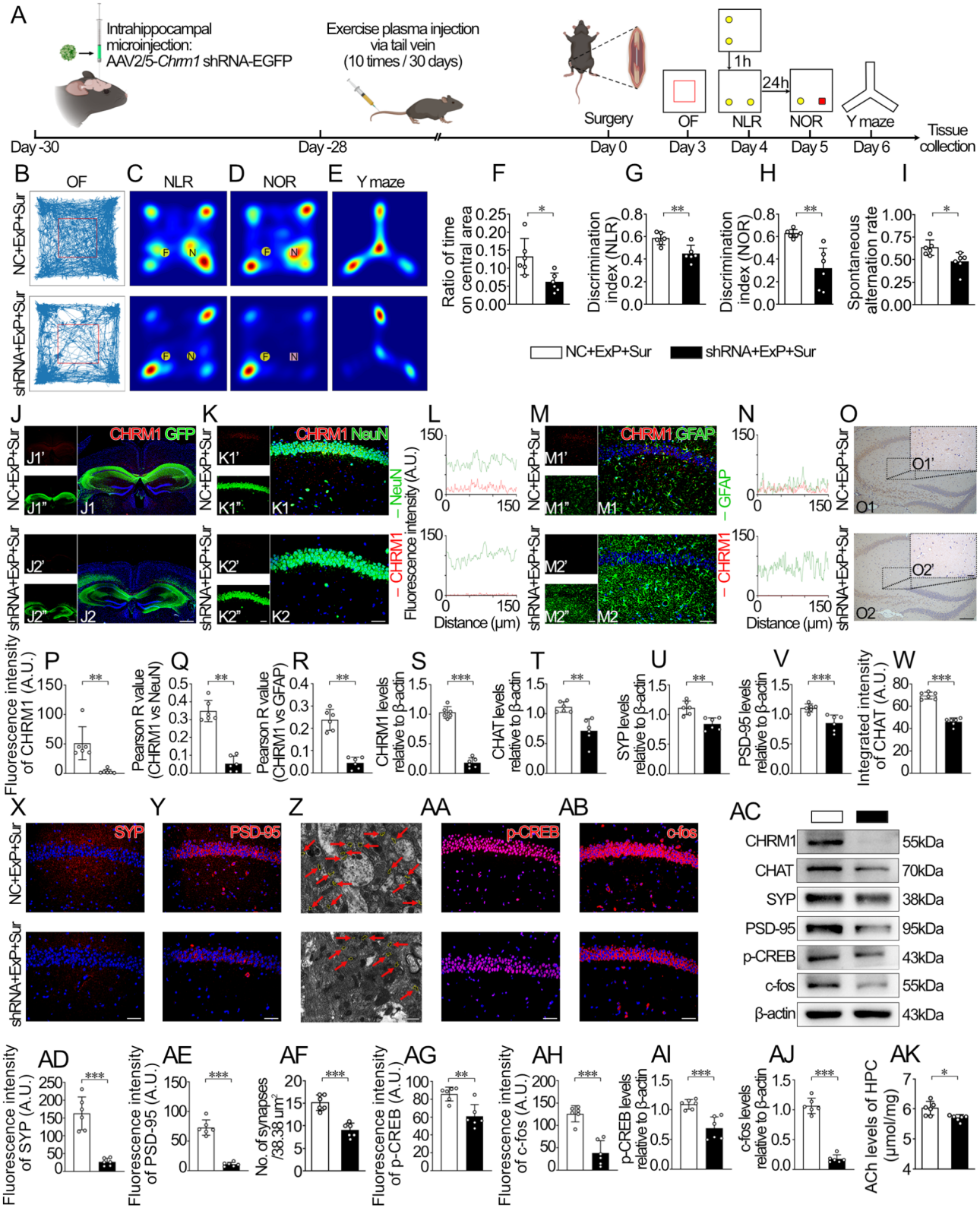

Fig. 10 (See legend on next page.)

(See figure on previous page.)

Fig. 10 AAV2/5-*Chrm1* shRNA silences *Chrm1*, reducing cognitive and synaptic recovery by exercise plasma. (**A**) Schematic illustration of the experimental design of intrahippocampal injection of AAV2/5-*Chrm1* shRNA-GFAP. (**B**, **F**) Representative locus diagrams and the statistical analyses of the OF tests. (**C**-**E**, **G**-**I**) Representative trajectory heat maps and the related statistical analyses of the NLR (**C**, **G**), NOR (**D**, **H**) and Y maze tests (**E**, **I**). (**J**, **P**) Representative images of the IF staining to evaluate the expressions of hippocampal GFP and CHRM1 (**J**), and the statistical analyses of the fluorescence intensity of hippocampal CHRM1 (**P**) in the hippocampal CA1 region. Scale bars: 50 μm. (**O**, **W**) Representative images of the IHC staining to evaluate the expressions of CHAT (**O**) in the hippocampal CA3 region and the related statistical analyses (**W**). Scale bars (O1-O2): 200 μm; (O1'-O2'): 50 μm. (**K**-**N**) Representative images of the IF staining to evaluate the colocalization of CHRM1 with NeuN (**K**), and CHRM1 with GFAP (**M**) in the hippocampal CA1 region, and the related lineplots of fluorescence intensity (**L**, **N**). Scale bars: 50 μm. (**S**-**V**, **AC**, **AI**-**AJ**) Representative Western blots of hippocampal CHRM1, CHAT, SYP, PSD-95, p-CREB and c-fos (**AC**), and the related statistical analyses (**S**-**V**, **AI**-**AJ**). (**X**-**Y**, **AA**-**AB**, **AD**-**AE**, **AG**-**AH**) Representative images of the IF staining to evaluate the expressions of SYP (**X**), PSD-95 (**Y**), p-CREB (**AA**) and c-fos (**AB**) in the hippocampal CA1 region and the related statistical analyses (**AD**-**AE**, **AG**-**AH**). Scale bars: 50 μm. (**Z**, **AF**) Representative TEM images of the hippocampal CA3 region with the synapses outlined in yellow and denoted by red arrows (**Z**) and the statistical analyses of synapse density (**AF**). Scale bars: 1 μm. (**Q**-**R**) Statistical analyses of the Pearson R value for the colocalization of CHRM1 with NeuN (**Q**) and CHRM1 with GFAP (**R**) in the hippocampal CA1 region. (**AK**) Statistical analyses of the levels of hippocampal ACh. Data are expressed as mean ± SD; $n = 6$ per group; * $P < 0.05$, ** $P < 0.01$, *** $P < 0.001$

The cognitive benefits of exercise plasma likely result from the combined action of multiple plasma factors rather than a single dominant factor. However, whether exercise-conditioned blood/plasma can replicate exercise-induced cognitive benefits under anesthesia and surgery remains undetermined. In this study, we found that systemic administration of plasma derived from mice undergoing 30-day running wheel training according to the exercise paradigms of this study mimicked the exercise-promoted restoration of postoperative HPC-dependent memory and HPC synaptic structure/function (Figs. 1 and 2), and inhibited neuroinflammatory responses to the surgical procedure by microglia and astrocytes (Fig. 3). These results extend previous studies on exercise-based interventions for POCD [15, 27] by offering a novel approach that addresses the limited capacity for perioperative exercise in elderly patients. Our study suggest that exercise-conditioned plasma can transfer the therapeutic benefits of exercise for POCD and associated neuropathological events to sedentary subjects, potentially benefiting elderly surgical patients at high risk of POCD.

BDNF, one of the best-established neurotrophins, is synthesized primarily in neurons across the brain, with particularly enriched expressions in the HPC and cortex [16]. Glial cells, especially astrocytes, can also contribute to BDNF production, typically upon stimulation [66]. BDNF functions as the pivotal regulator of synaptogenesis, synaptic plasticity, and cognition via its receptor TrkB. BDNF is highly responsive to stress and pathophysiological challenges [5]. Aged rodents are especially vulnerable to dysregulation of BDNF signaling pathways, leading to cognitive disorders. Furthermore, deficient BDNF/TrkB activity is involved in the pathogenesis of POCD. Previous rodent model studies have observed a decrease in BDNF levels and the activation level of its receptor TrkB in the brains of POCD model animals, paralleling cognitive impairment and synaptic dysfunction [5, 17]. In our study, we detected a similar anesthesia/surgery-induced decrease in total BDNF levels and TrkB activation within the HPC (Fig. 4). We propose that this widespread reduction in BDNF/TrkB signaling may be attributable to decreased BDNF synthesis in neurons and glial cells, potentially resulting from neuroinflammation secondary to anesthesia stress and surgery trauma (Fig. 3), as this neuroinflammatory state is characterized by neuronal dysfunction and abnormal glial reactivity with impaired neurotrophic effects [6, 10–14]. Additionally, the reduced hippocampal BDNF synthesis and release may be further exacerbated by affected activity of local neural circuits and innervation, such as the cholinergic neural circuit, which shows potential to enhance BDNF production (Fig. 9) but is susceptible to neuroinflammation (Fig. 7) [12, 46, 50].

Increasing evidence supports the notion that BDNF signaling contributes to exercise-induced cognitive benefits [28]. In healthy mice, exercise is confirmed to promote hippocampal-dependent learning and memory in a BDNF-dependent manner by activating the lactate/SIRT1/PCG1/FNDC5 pathway [29]. In mice at early stages of AD, hippocampal BDNF signaling is identified as an indispensable factor mediating the beneficial effects of exercise on cognition [30]. In some clinical trials, neuron-derived BDNF levels are even treated as biomarkers of cognitive improvement responsive to exercise [31]. In this study, we discovered that anesthesia/surgery-induced declines in BDNF distribution and BDNF-stimulated TrkB phosphorylation in hippocampal neurons, and potentially in astrocytes and microglia, were reversed by exercise and exercise-conditioned plasma similarly (Fig. 4). Changes in the distribution and potential responsiveness to hippocampal BDNF occurred in neurons and glial cells under surgical conditions, with or without exercise paradigms or exercise plasma administration. Neuronal BDNF distribution and responsiveness were positively related to synaptic formation, plasticity (Fig. 2), and cognitive status (Fig. 1), while glial BDNF distribution and potential reactivity showed a negative correlation to the proinflammatory activation or potentially detrimental phenotypes of glial cells (Fig. 3). These findings extend previous observations of decreased BDNF levels and TrkB activation in POCD models [5,

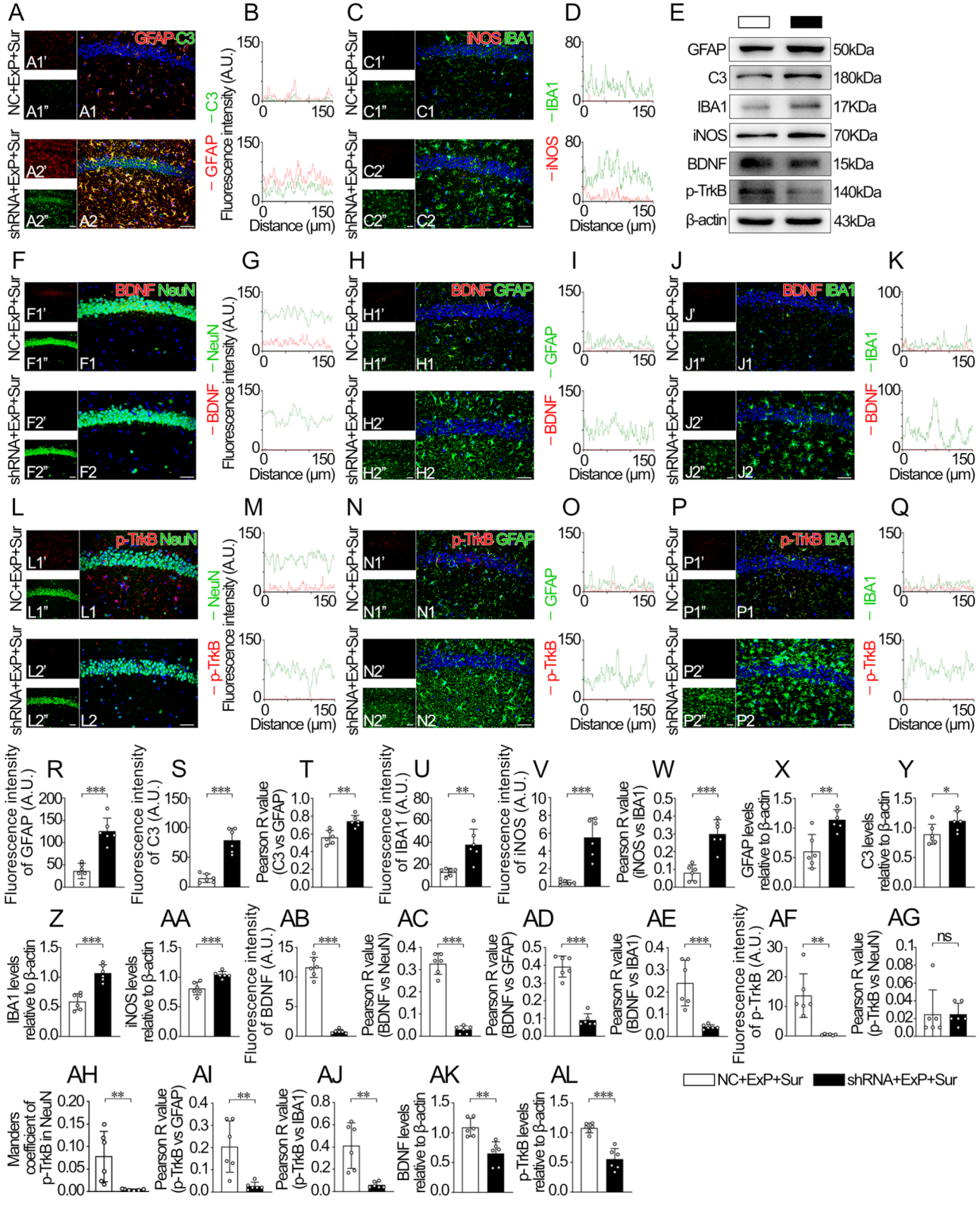

Fig. 11 (See legend on next page.)

(See figure on previous page.)

Fig. 11 AAV2/5-*Chrm1* shRNA silences *Chrm1*, reducing neuroinflammatory and BDNF/TrkB normalization by exercise plasma. (**A**-**D**, **F**-**Q**) Representative images of the IF staining to evaluate the colocalization of C3 with GFAP (**A**), and iNOS with IBA1 (**C**), BDNF with NeuN (**F**), BDNF with GFAP (**H**), BDNF with IBA1 (**J**), p-TrkB (Tyr816) with NeuN (**L**), p-TrkB (Tyr816) with GFAP (**N**) and p-TrkB (Tyr816) with IBA1 (**P**) in the hippocampal CA1 region, and the related lineplots of fluorescence intensity (**B**, **D**, **G**, **I**, **K**, **M**, **O**, **Q**). Scale bars: 50 μm. (**E**, **X**-**AA**, **AK**-**AL**) Representative Western blots of hippocampal C3, GFAP, iNOS, IBA1, BDNF and p-TrkB (Tyr816) (**E**), and the related statistical analyses (**X**-**AA**, **AK**-**AL**). (**R**-**S**, **U**-**V**, **AB**, **AF**) Statistical analyses of the total fluorescence intensity of GFAP (**R**), C3 (**S**), IBA1 (**U**), iNOS (**V**), BDNF (**AB**) and p-TrkB (Tyr816) (**AF**) in the hippocampal CA1 region. (**T**, **W**, **AC**-**AE**, **AG**, **AI**-**AJ**) Statistical analyses of the Pearson R value for the colocalization of C3 with GFAP (**T**), iNOS with IBA1 (**W**), BDNF with NeuN (**AC**), BDNF with GFAP (**AD**), BDNF with IBA1 (**AE**), p-TrkB (Tyr816) with NeuN (**AG**), p-TrkB (Tyr816) with GFAP (**AI**), and p-TrkB (Tyr816) with IBA1 (**AJ**) in the hippocampal CA1 region. (**AH**) Statistical analyses of the Manders coefficient of the colocalization of p-TrkB (Tyr816) with NeuN in the hippocampal CA1 region. Data are expressed as mean ± SD; $n = 6$ per group; ns, nonsignificant, * $P < 0.05$, ** $P < 0.01$, *** $P < 0.001$

17] by providing a more detailed characterization of BDNF/TrkB signaling changes across different cell types and their relationship to neuroinflammation and cognitive outcomes. To further investigate whether BDNF signaling mediates the benefits of exercise-conditioned plasma, in this study, TrkB was pharmacologically inhibited with ANA-12 (Fig. 5A), a blood–brain barrier-permeable, highly selective TrkB antagonist routinely used in animal studies [46, 67, 73]. ANA-12 specifically binds and potently inhibits TrkB rather than TrkA or TrkC [74]. To address potential off-target effects, we included an ANA12+Ex+Sur group to compare the effects of ANA-12 on voluntary exercise training (Fig. S5-S6). As expected, ANA-12 administration attenuated the exercise-conditioned plasma-induced neuronal BDNF distribution and activation of BDNF/TrkB signaling, as well as potential effects on glial cells (Fig. 5J-AF), consequently abolishing the therapeutic effects on postoperative cognitive impairment (Fig. 5B-I) and the associated hippocampal synaptic deficits and neuroinflammation (Fig. 6). Similar effects were observed in the ANA12+Ex+Sur group (Fig. S5-S6), further supporting the specificity of ANA-12 in targeting TrkB signaling. These data support the autocrine and paracrine regulation of hippocampal BDNF and the role of BDNF/TrkB signaling as the critical mediator of neuroprotection by exercise plasma under conditions of POCD. Intriguingly, while BDNF has been shown to alleviate neuroinflammation in models of diabetes and radiation-induced brain injury [75, 76], the present study provides evidence for potential anti-neuroinflammatory effects of the BDNF/TrkB pathway in the context of POCD for the first time. This is suggested by the reverse correlation of BDNF expression and TrkB activation with glial inflammatory responses (Figs. 4 and 5), as well as the reemergence of hippocampal neuroinflammation following TrkB blockage (Fig. 6N-Q, T-AD). It's important to note that while the distribution of full-length TrkB in glial cells, particularly microglia, remains a subject of ongoing research [66, 77, 78], our findings indicate a potential role for BDNF/TrkB signaling in modulating neuroinflammatory responses in the POCD context, addressing a gap in our understanding of POCD pathology.

The MS-hippocampal circuit is crucial for encoding and consolidating HPC-dependent memory [40]. During memory tasks, increased ACh release in the HPC is observed [41]. Blocking hippocampal mAChRs and α7 nAChRs receptors, either through cholinergic receptor antagonists or genetic knockout, leads to cognitive deficits in mice [42]. Positive modulation of CHRM1 enhances cognitive flexibility in primates [43]. Mechanistically, basal forebrain cholinergic input modulates hippocampal functions and synaptic plasticity by maintaining high ACh levels, which suppresses abnormal network activity, promotes theta oscillations, enhances signal-to-noise ratio, stabilizes GluA1 receptors, and boosts axonal excitability [44, 45]. Additionally, cholinergic activity activates BDNF signaling through astrocytic CHRM1, preserving contextual memory [46]. Dysfunction in this circuit is linked to neurodegenerative and neuroinflammatory diseases, presenting potential therapeutic targets. Enhancing cholinergic signaling can slow prion neurodegeneration and restore memory loss [47]. Photoactivation of MS-CA1 cholinergic inputs during memory consolidation rescues tau-induced spatial memory deficits in a θ rhythm-dependent manner [48]. Cholinomimetic drugs alleviate neuroinflammation, sustain synapses, and improve cognition in AD models [49]. In sepsis-associated encephalopathy and surgery-induced delirium models, selective activation of hippocampal cholinergic innervation restores synaptic plasticity and memory, suggesting neuroprotective effects under systemic inflammation [12, 50]. Exercise and blood factors also benefit the hippocampal cholinergic network in aging and neurodegenerative conditions. Exercise re-emerges the MS cholinergic phenotype, restores ACh efflux, and reverses age-related declines in hippocampal fibers and cognitive behaviors [51–53]. Our previous study proposed that blood from young mice (3-month-old) improves hippocampal cholinergic activity and AD-like pathology [54], though the effects of exercise-conditioned blood on postoperative cholinergic defects remain unclear. In this study, we found that postoperative defects in the MS-hippocampal cholinergic circuit, characterized by decreases in $CHAT^+$ cholinergic neurons within the MS and $CHAT^+$ cholinergic afferent fibers, neuronal and astroglial expressions of CHRM1,

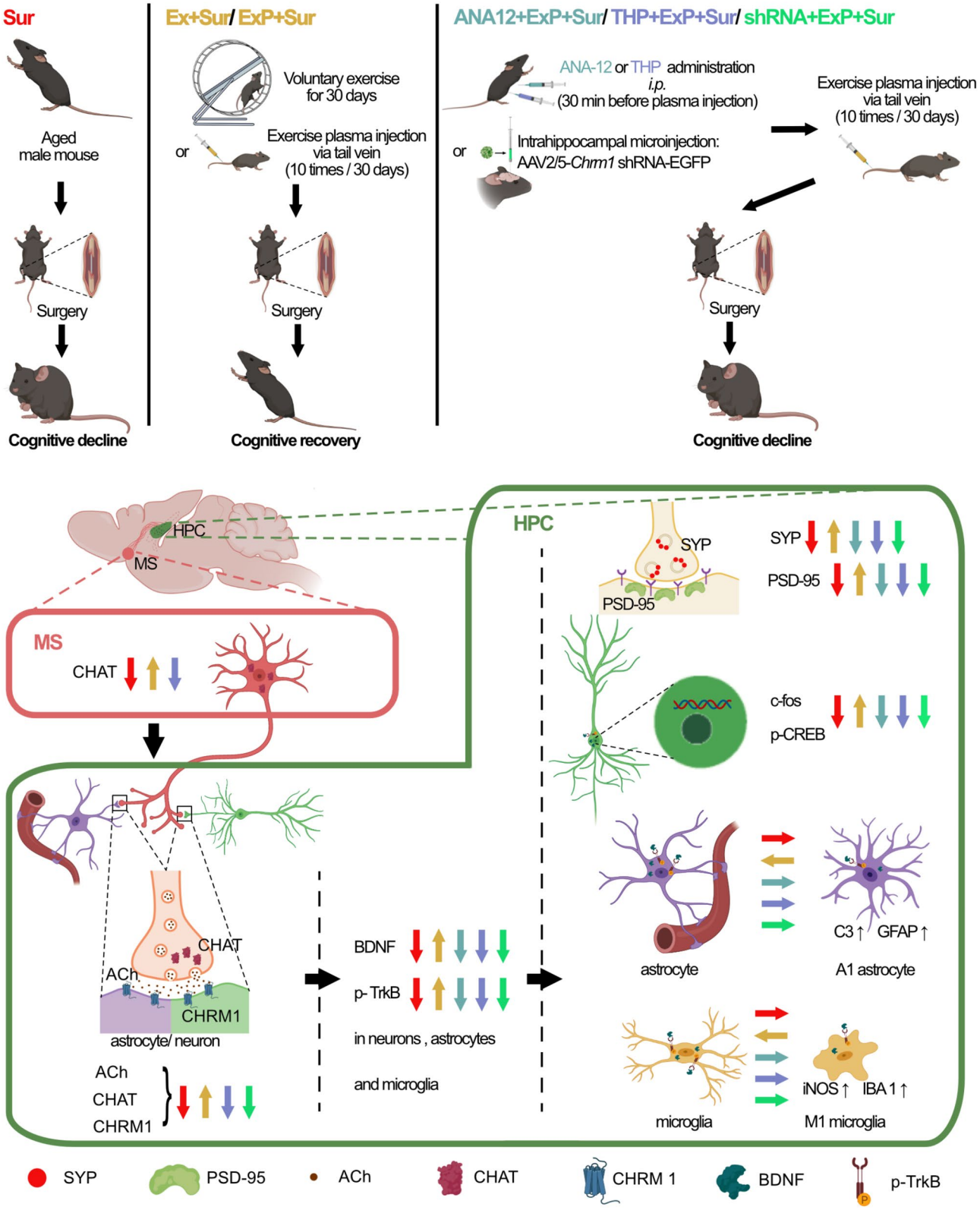

Fig. 12 Exercise-conditioned plasma benefits POCD via CHRM1-dependent hippocampal cholinergic activity-regulated BDNF/TrkB signaling

and ACh release within the HPC, were normalized by exercise on a running wheel or intravenous infusion of exercise-conditioned plasma (Fig. 7). Given no evident changes in cell density detected in the MS (Fig. 7B),

which is not the niche of adult neurogenesis, the down-regulated CHAT level within the MS following surgery might be attributable to the loss of the $CHAT^+$ phenotype rather than rapid cell death [51, 52]. The deteriorated CHAT expression and degeneration of MS cholinergic neurons were accompanied by dysfunction in projection to the HPC (Fig. 7A, C). This dysfunction could be reversed by chronic exposure to prolonged exercise or exercise plasma-induced neurotrophic/neuroprotective microenvironment. CHRM1, a well-established hippocampal cholinergic receptor, is involved in cognitive mechanisms [43, 46] and mediates the neuroprotection of youthful blood factors in AD [54]. Our results show that CHRM1 was altered by surgery, exercise, and exercise plasma (Fig. 7E-N) in parallel with cognition (Fig. 1) and synaptic deficits (Figs. 2 and 3). Thus, CHRM1 was selected as one of the major targets in this study. We pharmacologically blocked its activity using THP (Fig. 8A), an antagonist with high affinity and specificity for CHRM1, capable of crossing the blood-brain barrier, and without risks of cognitive disturbance [68]. THP is not only a reliable tool for studying CHRM1-mediated cholinergic transmission but also an FDA-approved medication for managing Parkinsonism symptoms [79]. To validate THP specificity and exclude potential off-target effects, we included a THP+Ex+Sur group to compare the effects of THP on regular exercise training (Fig. S9-S10). Additionally, we silenced hippocampal *Chrm1* expression in vivo through intrahippocampal injection of AAV vectors expressing *Chrm1* shRNA (Fig. 10A). As anticipated, pharmacological antagonism (Figs. 8 and 9) or in vivo knockdown targeting CHRM1 (Figs. 10 and 11) abrogated the exercise plasma-boosted restoration of hippocampal synaptogenesis, synaptic plasticity, and the inhibition of neuroinflammatory reaction by glial cells following anesthesia and surgery, resulting in the failure of cognitive recovery. The consistent results observed between the THP+ExP+Sur and THP+Ex+Sur groups not only rule out potential off-target effects of THP but also reinforce the critical role of CHRM1 in mediating the cognitive benefits induced by both exercise-conditioned plasma and regular exercise. Collectively, these findings prove that CHRM1-mediated hippocampal cholinergic activity at least partly underlies the therapeutic effects of exercise-conditioned plasma on postoperative cognitive impairments and related pathological changes (Fig. 12). Interestingly, the consistency of hippocampal cholinergic innervation with CHRM1 levels and the THP administration or *Chrm1* silencing-induced decrease in hippocampal cholinergic fibers and ACh levels observed in this study might provide novel evidence for cholinergic receptor-guided axon targeting within the HPC [80]. Concerning molecular mechanisms, our data reveal a novel role of hippocampal cholinergic activity in anti-neuroinflammation and regulating BDNF/TrkB signaling in the context of POCD (Fig. 12). This is evidenced by positive correlations between hippocampal cholinergic activity and BDNF/TrkB signaling, and the attenuated exercise plasma-promoted BDNF distribution and TrkB activation in hippocampal neurons, with potential effects on glial cells, by cholinergic antagonism or *Chrm1* knockdown (Figs. 9 and 11). While previous studies have shown the involvement of cholinergic signaling in cognitive function and neuroplasticity [12], our findings extend this understanding by demonstrating the roles of specific cholinergic receptor (CHRM1)-dependent hippocampal cholinergic activity in modulating neuroinflammation and BDNF/TrkB signaling in POCD. This provides a more comprehensive mechanistic insight into how cholinergic activity contributes to cognitive recovery in the postoperative context, offering potential new targets for POCD prevention and treatment.

Despite demonstrating the protective effects of exercise-conditioned plasma on hippocampal-dependent learning, memory, and associated pathology under surgical conditions, and elucidating the role of the MS-hippocampal circuit and BDNF/TrkB signaling, this study has several limitations: (1) The study included only 16-17-month-old male C57BL/6J mice, leaving the effects of sex, species, and strains variations unexplored. (2) While we examined the brain cell and cholinergic circuit responses to exercise and exercise-conditioned plasma, the exercise-induced alterations in plasma components underlying neuroprotection in the context of POCD require further investigation. (3) Future studies should explore the molecular mechanisms driving the exercise/exercise plasma-induced increase in hippocampal CHRM1 expression and cholinergic innervation. innervation. (4) The precise mechanisms of BDNF's effects on various cell types, especially glial cells, warrant additional research. Our BDNF staining results indicate protein distribution but not necessarily synthesis. Moreover, the functional significance of full-length TrkB in astrocytes and microglia within the context of POCD and exercise/exercise-conditioned plasma intervention needs further exploration.

Conclusion

In summary, our data indicate that exercise-conditioned plasma mimics the protection by exercise against anesthesia/surgery-induced neuroinflammation, synaptic deficits, and cognitive decline, at least partly, by CHRM1-dependent hippocampal cholinergic activity-regulated BDNF/TrkB signaling.

Abbreviations

AAV	Adeno-associated virus
Ach	Acetylcholine
AD	Alzheimer's disease

BDNF	Brain-derived neurotrophic factor
BFCNs	Basal forebrain cholinergic neurons
C3	Complement component 3
CHAT	Choline acetyltransferase
CHRM1	Cholinergic receptor muscarinic 1
CREB	cAMP response element-binding protein
Con	Control
DB	Diagonal band
Ex	Exercise
ExP	Exercise Plasma
GFAP	Glial fibrillary acidic protein
HPC	Hippocampus
i.p.	Intraperitoneal
IBA1	Ionized calcium-binding adapter molecule 1
IF	Immunofluorescence
IHC	Immunohistochemistry
iNOS	Inducible nitric oxide synthase
LTP	Long-term potentiation
mAChRs	Muscarinic acetylcholine receptors
MS	Medial septum
nAChRs	Nicotinic acetylcholine receptors
NLR	Novel location recognition
NOR	Novel object recognition
OF	Open field
p-CREB	Phosphorylated CREB
PFC	Prefrontal cortex
POCD	Postoperative cognitive dysfunction
PSD-95	Postsynaptic density protein 95
Sur	Surgery
SYP	Synaptophysin
TEM	Transmission electron microscopy
THP	Trihexyphenidyl
TrkB	Tropomyosin receptor kinase B

Supplementary Information

The online version contains supplementary material available at https://doi.org/10.1186/s12964-024-01938-7.

Supplementary Material 1

Supplementary Material 2

Acknowledgements
We thank Prof. Shouchen Zhang from Harbin Medical University for the technical assistance.

Author contributions
X. L., W. X., Y. L. and M. L. performed the behavioral tests. X. L., W. X., Y. L. and X. Y. conduced the histopathological tests. X.L., W.X., F. X., and W. G. carried out the molecular and biochemical tests. X. L., W. X. and Z. C. analyzed the data. X. L. and L. S. drafted the manuscript. G. W., L. S. and S. W. designed and guided the study. All authors have reviewed and approved the final manuscript.

Funding
This study was supported by the National Natural Science Foundation ofChina (Grant number 82172192 to GW; 82003392 to LS).

Data availability
No datasets were generated or analysed during the current study.

Declarations

Ethic approval and consent to participate
All animal handling and use in this study were approved by Institutional Research Board of Harbin Medical University (No. HMUIRB2023016).

Consent for publication
Not applicable.

Competing interests
The authors declare no competing interests.

Author details
[1]Department of Anesthesiology, Harbin Medical University Cancer Hospital, Harbin 150081, China
[2]Department of Human Anatomy, School of Basic Medicine, Harbin Medical University, Harbin 150081, China
[3]Department of Anesthesiology, The Fourth Affiliated Hospital of Harbin Medical University, Harbin 150001, China

Received: 18 June 2024 / Accepted: 10 November 2024
Published online: 18 November 2024

References

1. Vlisides PE, Li D, Maywood M, Zierau M, Lapointe AP, Brooks J, McKinney AM, Leis AM, Mentz G, Mashour GA. Electroencephalographic biomarkers, cerebral oximetry, and postoperative cognitive function in adult Noncardiac Surgical patients: a prospective cohort study. Anesthesiology. 2023;139:568–79.
2. Olotu C, Ascone L, Wiede J, Manthey J, Kuehn S, Scherwath A, Kiefmann R. The effect of delirium preventive measures on the occurrence of postoperative cognitive dysfunction in older adults undergoing cardiovascular surgery. The DelPOCD randomised controlled trial. J Clin Anesth. 2022;78:110686.
3. Zhou Y, Ju H, Hu Y, Li T, Chen Z, Si Y, Sun X, Shi Y, Fang H. Tregs dysfunction aggravates postoperative cognitive impairment in aged mice. J Neuroinflammation. 2023;20:75.
4. Evered L, Silbert B, Knopman DS, Scott DA, DeKosky ST, Rasmussen LS, Oh ES, Crosby G, Berger M, Eckenhoff RG. Nomenclature Consensus Working G: recommendations for the nomenclature of cognitive change associated with anaesthesia and surgery-2018. Br J Anaesth. 2018;121:1005–12.
5. Muscat SM, Deems NP, Butler MJ, Scaria EA, Bettes MN, Cleary SP, Bockbrader RH, Maier SF, Barrientos RM. Selective TLR4 antagonism prevents and reverses Morphine-Induced Persistent Postoperative Cognitive Dysfunction, Dysregulation of synaptic elements, and impaired BDNF signaling in aged male rats. J Neurosci. 2023;43:155–72.
6. Liu Q, Sun YM, Huang H, Chen C, Wan J, Ma LH, Sun YY, Miao HH, Wu YQ. Sirtuin 3 protects against anesthesia/surgery-induced cognitive decline in aged mice by suppressing hippocampal neuroinflammation. J Neuroinflammation. 2021;18:41.
7. Borchers F, Spies CD, Feinkohl I, Brockhaus WR, Kraft A, Kozma P, Fislage M, Kuhn S, Ionescu C, Speidel S, et al. Methodology of measuring postoperative cognitive dysfunction: a systematic review. Br J Anaesth. 2021;126:1119–27.
8. Yang X, Huang X, Li M, Jiang Y, Zhang H. Identification of individuals at risk for postoperative cognitive dysfunction (POCD). Ther Adv Neurol Disord. 2022;15:17562864221114356.
9. Liu Y, Fu H, Wang T. Neuroinflammation in perioperative neurocognitive disorders: from bench to the bedside. CNS Neurosci Ther. 2022;28:484–96.
10. Paolicelli RC, Sierra A, Stevens B, Tremblay ME, Aguzzi A, Ajami B, Amit I, Audinat E, Bechmann I, Bennett M, et al. Microglia states and nomenclature: a field at its crossroads. Neuron. 2022;110:3458–83.
11. Cahill MK, Collard M, Tse V, Reitman ME, Etchenique R, Kirst C, Poskanzer KE. Network-level encoding of local neurotransmitters in cortical astrocytes. Nature. 2024;629:146–53.
12. Wang T, Xu G, Zhang X, Ren Y, Yang T, Xiao C, Zhou C. Malfunction of astrocyte and cholinergic input is involved in postoperative impairment of hippocampal synaptic plasticity and cognitive function. Neuropharmacology. 2022;217:109191.
13. Escartin C, Galea E, Lakatos A, O'Callaghan JP, Petzold GC, Serrano-Pozo A, Steinhauser C, Volterra A, Carmignoto G, Agarwal A, et al. Reactive astrocyte nomenclature, definitions, and future directions. Nat Neurosci. 2021;24:312–25.
14. He L, Duan X, Li S, Zhang R, Dai X, Lu M. Unveiling the role of astrocytes in postoperative cognitive dysfunction. Ageing Res Rev. 2024;95:102223.
15. Liu Y, Chu JMT, Ran Y, Zhang Y, Chang RCC, Wong GTC. Prehabilitative resistance exercise reduces neuroinflammation and improves mitochondrial health in aged mice with perioperative neurocognitive disorders. J Neuroinflammation. 2022;19:150.
16. Wang CS, Kavalali ET, Monteggia LM. BDNF signaling in context: from synaptic regulation to psychiatric disorders. Cell. 2022;185:62–76.

17. Nemoto A, Goyagi T, Nemoto W, Nakagawasai O, Tan-No K, Niiyama Y. Low skeletal muscle Mass is Associated with Perioperative Neurocognitive Disorder due to decreased neurogenesis in rats. Anesth Analg. 2022;134:194–203.
18. Chen Y, Joo J, Chu JM, Chang RC, Wong GT. Downregulation of the glucose transporter GLUT 1 in the cerebral microvasculature contributes to postoperative neurocognitive disorders in aged mice. J Neuroinflammation. 2023;20:237.
19. Erickson KI, Donofry SD, Sewell KR, Brown BM, Stillman CM. Cognitive aging and the Promise of Physical Activity. Annu Rev Clin Psychol. 2022;18:417–42.
20. Islam MR, Valaris S, Young MF, Haley EB, Luo R, Bond SF, Mazuera S, Kitchen RR, Caldarone BJ, Bettio LEB, et al. Exercise hormone irisin is a critical regulator of cognitive function. Nat Metab. 2021;3:1058–70.
21. Tang C, Liu M, Zhou Z, Li H, Yang C, Yang L, et al. Treadmill exercise alleviates cognition disorder by activating the FNDC5: dual role of integrin alphaV/beta5 in Parkinson's Disease. Int J Mol Sci. 2023;24:7830.
22. Marino G, Campanelli F, Natale G, De Carluccio M, Servillo F, Ferrari E, Gardoni F, Caristo ME, Picconi B, Cardinale A, et al. Intensive exercise ameliorates motor and cognitive symptoms in experimental Parkinson's disease restoring striatal synaptic plasticity. Sci Adv. 2023;9:eadh1403.
23. Casaletto KB, Staffaroni AM, Wolf A, Appleby B, Brushaber D, Coppola G, Dickerson B, Domoto-Reilly K, Elahi FM, Fields J, et al. Active lifestyles moderate clinical outcomes in autosomal dominant frontotemporal degeneration. Alzheimers Dement. 2020;16:91–105.
24. Khan MB, Alam H, Siddiqui S, Shaikh MF, Sharma A, Rehman A, Baban B, Arbab AS, Hess DC. Exercise improves cerebral blood Flow and Functional outcomes in an experimental mouse model of vascular cognitive impairment and dementia (VCID). Transl Stroke Res. 2024;15:446–61.
25. Riggs L, Piscione J, Laughlin S, Cunningham T, Timmons BW, Courneya KS, Bartels U, Skocic J, de Medeiros C, Liu F, et al. Exercise training for neural recovery in a restricted sample of pediatric brain tumor survivors: a controlled clinical trial with crossover of training versus no training. Neuro Oncol. 2017;19:440–50.
26. Lange M, Joly F, Vardy J, Ahles T, Dubois M, Tron L, Winocur G, De Ruiter MB, Castel H. Cancer-related cognitive impairment: an update on state of the art, detection, and management strategies in cancer survivors. Ann Oncol. 2019;30:1925–40.
27. Lai Z, Shan W, Li J, Min J, Zeng X, Zuo Z. Appropriate exercise level attenuates gut dysbiosis and valeric acid increase to improve neuroplasticity and cognitive function after surgery in mice. Mol Psychiatry. 2021;26:7167–87.
28. Bieri G, Schroer AB, Villeda SA. Blood-to-brain communication in aging and rejuvenation. Nat Neurosci. 2023;26:379–93.
29. El Hayek L, Khalifeh M, Zibara V, Abi Assaad R, Emmanuel N, Karnib N, El-Ghandour R, Nasrallah P, Bilen M, Ibrahim P, et al. Lactate mediates the effects of Exercise on Learning and Memory through SIRT1-Dependent activation of hippocampal brain-derived neurotrophic factor (BDNF). J Neurosci. 2019;39:2369–82.
30. Choi SH, Bylykbashi E, Chatila ZK, Lee SW, Pulli B, Clemenson GD, et al. Combined adult neurogenesis and BDNF mimic exercise effects on cognition in an Alzheimer's mouse model. Science. 2018;361:eaan8821.
31. Delgado-Peraza F, Nogueras-Ortiz C, Simonsen AH, Knight DD, Yao PJ, Goetzl EJ, Jensen CS, Hogh P, Gottrup H, Vestergaard K, et al. Neuron-derived extracellular vesicles in blood reveal effects of exercise in Alzheimer's disease. Alzheimers Res Ther. 2023;15:156.
32. Han H, Zhao Y, Du J, Wang S, Yang X, Li W, Song J, Zhang S, Zhang Z, Tan Y, et al. Exercise improves cognitive dysfunction and neuroinflammation in mice through histone H3 lactylation in microglia. Immun Ageing. 2023;20:63.
33. Feng S, Wu C, Zou P, Deng Q, Chen Z, Li M, Zhu L, Li F, Liu TC, Duan R, Yang L. High-intensity interval training ameliorates Alzheimer's disease-like pathology by regulating astrocyte phenotype-associated AQP4 polarization. Theranostics. 2023;13:3434–50.
34. Horowitz AM, Fan X, Bieri G, Smith LK, Sanchez-Diaz CI, Schroer AB, Gontier G, Casaletto KB, Kramer JH, Williams KE, Villeda SA. Blood factors transfer beneficial effects of exercise on neurogenesis and cognition to the aged brain. Science. 2020;369:167–73.
35. De Miguel Z, Khoury N, Betley MJ, Lehallier B, Willoughby D, Olsson N, Yang AC, Hahn O, Lu N, Vest RT, et al. Exercise plasma boosts memory and dampens brain inflammation via clusterin. Nature. 2021;600:494–9.
36. Leiter O, Brici D, Fletcher SJ, Yong XLH, Widagdo J, Matigian N, Schroer AB, Bieri G, Blackmore DG, Bartlett PF, et al. Platelet-derived exerkine CXCL4/platelet factor 4 rejuvenates hippocampal neurogenesis and restores cognitive function in aged mice. Nat Commun. 2023;14:4375.
37. Wei W, Riley NM, Lyu X, Shen X, Guo J, Raun SH, Zhao M, Moya-Garzon MD, Basu H, Sheng-Hwa Tung A et al. Organism-wide, cell-type-specific secretome mapping of exercise training in mice. Cell Metab. 2023, 35: 1261–1279 e1211.
38. Ananth MR, Rajebhosale P, Kim R, Talmage DA, Role LW. Basal forebrain cholinergic signalling: development, connectivity and roles in cognition. Nat Rev Neurosci. 2023;24:233–51.
39. Li X, Yu H, Zhang B, Li L, Chen W, Yu Q, Huang X, Ke X, Wang Y, Jing W, et al. Molecularly defined and functionally distinct cholinergic subnetworks. Neuron. 2022;110:3774–e37883777.
40. He G, Li Y, Deng H, Zuo H. Advances in the study of cholinergic circuits in the central nervous system. Ann Clin Transl Neurol. 2023;10:2179–91.
41. Teles-Grilo Ruivo LM, Baker KL, Conway MW, Kinsley PJ, Gilmour G, Phillips KG, Isaac JTR, Lowry JP, Mellor JR. Coordinated Acetylcholine Release in Prefrontal Cortex and Hippocampus is Associated with Arousal and reward on distinct timescales. Cell Rep. 2017;18:905–17.
42. Gu Z, Stevanovic KD, Cushman JD, Yakel JL. Cholinergic-sensitive Theta oscillations in Memory Encoding in mice. J Neurosci. 2024;44:e1313232024.
43. Hassani SA, Neumann A, Russell J, Jones CK, Womelsdorf T. M(1)-selective muscarinic allosteric modulation enhances cognitive flexibility and effective salience in nonhuman primates. Proc Natl Acad Sci U S A. 2023;120:e2216792120.
44. Ma X, Zhang Y, Wang L, Li N, Barkai E, Zhang X, Lin L, Xu J. The Firing of Theta State-related septal cholinergic neurons disrupt hippocampal Ripple oscillations via Muscarinic receptors. J Neurosci. 2020;40:3591–603.
45. Ballinger EC, Ananth M, Talmage DA, Role LW. Basal Forebrain Cholinergic circuits and Signaling in Cognition and Cognitive decline. Neuron. 2016;91:1199–218.
46. Li WP, Su XH, Hu NY, Hu J, Li XW, Yang JM, Gao TM. Astrocytes mediate cholinergic regulation of adult hippocampal neurogenesis and memory through M(1) muscarinic receptor. Biol Psychiatry. 2022;92:984–98.
47. Bradley SJ, Bourgognon JM, Sanger HE, Verity N, Mogg AJ, White DJ, Butcher AJ, Moreno JA, Molloy C, Macedo-Hatch T, et al. M1 muscarinic allosteric modulators slow prion neurodegeneration and restore memory loss. J Clin Invest. 2017;127:487–99.
48. Wu D, Yu N, Gao Y, Xiong R, Liu L, Lei H, Jin S, Liu J, Liu Y, Xie J, et al. Targeting a vulnerable septum-hippocampus cholinergic circuit in a critical time window ameliorates tau-impaired memory consolidation. Mol Neurodegener. 2023;18:23.
49. Munafo A, Cantone AF, Di Benedetto G, Torrisi SA, Burgaletto C, Bellanca CM, Gaudio G, Broggi G, Caltabiano R, Leggio GM, et al. Pharmacological enhancement of cholinergic neurotransmission alleviates neuroinflammation and improves functional outcomes in a triple transgenic mouse model of Alzheimer's disease. Front Pharmacol. 2024;15:1386224.
50. Yin L, Zhang J, Ma H, Zhang X, Fan Z, Yang Y, Li M, Han J, Zhang X. Selective activation of cholinergic neurotransmission from the medial septal nucleus to hippocampal pyramidal neurones improves sepsis-induced cognitive deficits in mice. Br J Anaesth. 2023;130:573–84.
51. Hall JM, Savage LM. Exercise leads to the re-emergence of the cholinergic/nestin neuronal phenotype within the medial septum/diagonal band and subsequent rescue of both hippocampal ACh efflux and spatial behavior. Exp Neurol. 2016;278:62–75.
52. Hall JM, Gomez-Pinilla F, Savage LM. Nerve growth factor is responsible for Exercise-Induced Recovery of Septohippocampal Cholinergic structure and function. Front Neurosci. 2018;12:773.
53. Teglas T, Nemeth Z, Koller A, Van der Zee EA, Luiten PGM, Nyakas C. Effects of Long-Term Moderate Intensity Exercise on cognitive behaviors and cholinergic forebrain in the aging rat. Neuroscience. 2019;411:65–75.
54. Xia E, Xu F, Hu C, Kumal JPP, Tang X, Mao D, Li Y, Wu D, Zhang R, Wu S, Sun L. Young blood rescues the cognition of Alzheimer's Model mice by restoring the Hippocampal Cholinergic Circuit. Neuroscience. 2019;417:57–69.
55. Lazarov O, Robinson J, Tang YP, Hairston IS, Korade-Mirnics Z, Lee VM, Hersh LB, Sapolsky RM, Mirnics K, Sisodia SS. Environmental enrichment reduces Abeta levels and amyloid deposition in transgenic mice. Cell. 2005;120:701–13.
56. Endo F, Kasai A, Soto JS, Yu X, Qu Z, Hashimoto H, Gradinaru V, Kawaguchi R, Khakh BS. Molecular basis of astrocyte diversity and morphology across the CNS in health and disease. Science. 2022;378:eadc9020.
57. Lugo JN, Smith GD, Arbuckle EP, White J, Holley AJ, Floruta CM, Ahmed N, Gomez MC, Okonkwo O. Deletion of PTEN produces autism-like behavioral deficits and alterations in synaptic proteins. Front Mol Neurosci. 2014;7:27.

58. Smith GD, White J, Lugo JN. Superimposing Status Epilepticus on Neuron Subset-Specific PTEN Haploinsufficient and Wild Type mice results in long-term changes in Behavior. Sci Rep. 2016;6:36559.
59. Simmons DA, Lartey FM, Schuler E, Rafat M, King G, Kim A, Ko R, Semaan S, Gonzalez S, Jenkins M, et al. Reduced cognitive deficits after FLASH irradiation of whole mouse brain are associated with less hippocampal dendritic spine loss and neuroinflammation. Radiother Oncol. 2019;139:4–10.
60. Richetin K, Leclerc C, Toni N, Gallopin T, Pech S, Roybon L, Rampon C. Genetic manipulation of adult-born hippocampal neurons rescues memory in a mouse model of Alzheimer's disease. Brain. 2015;138:440–55.
61. Lueptow LM. Novel object Recognition Test for the investigation of learning and memory in mice. J Vis Exp. 2017;126:55718.
62. Du Z, Song Y, Chen X, Zhang W, Zhang G, Li H, Chang L, Wu Y. Knockdown of astrocytic Grin2a aggravates beta-amyloid-induced memory and cognitive deficits through regulating nerve growth factor. Aging Cell. 2021;20:e13437.
63. Rao SR, Olechnowicz SWZ, Kratschmer P, Jepson JEC, Edwards CM, Edwards JR. Small animal video tracking for activity and path analysis using a Novel Open-Source Multi-platform Application (AnimApp). Sci Rep. 2019;9:12343.
64. Schroer AB, Ventura PB, Sucharov J, Misra R, Chui MKK, Bieri G, Horowitz AM, Smith LK, Encabo K, Tenggara I, et al. Platelet factors attenuate inflammation and rescue cognition in ageing. Nature. 2023;620:1071–9.
65. Wan J, Ma L, Jiao X, Dong W, Lin J, Qiu Y, Wu W, Liu Q, Chen C, Huang H, et al. Impaired synaptic plasticity and decreased excitability of hippocampal glutamatergic neurons mediated by BDNF downregulation contribute to cognitive dysfunction in mice induced by repeated neonatal exposure to ketamine. CNS Neurosci Ther. 2024;30:e14604.
66. Esvald EE, Tuvikene J, Kiir CS, Avarlaid A, Tamberg L, Sirp A, Shubina A, Cabrera-Cabrera F, Pihlak A, Koppel I, et al. Revisiting the expression of BDNF and its receptors in mammalian development. Front Mol Neurosci. 2023;16:1182499.
67. Sun YX, Su YA, Wang Q, Zheng JY, Zhang CC, Wang T, Liu X, Ma YN, Li XX, Zhang XQ, et al. The causal involvement of the BDNF-TrkB pathway in dentate gyrus in early-life stress-induced cognitive deficits in male mice. Transl Psychiatry. 2023;13:173.
68. Zhou JC, Jiang JB, Guo H, Yang SR, Liu CF, Qu WM, Huang ZL, Ding FF. Trihexyphenidyl increases delta activity in non-rapid eye movement sleep without impairing cognitive function in rodent models. Neuropharmacology. 2022;218:109217.
69. Xiong C, Zhang Z, Baht GS, Terrando N. A mouse model of orthopedic surgery to study postoperative cognitive dysfunction and tissue regeneration. J Vis Exp. 2018;132:56701.
70. Chen K, Hu Q, Xie Z, Yang G. Monocyte NLRP3-IL-1beta hyperactivation mediates neuronal and synaptic dysfunction in Perioperative Neurocognitive Disorder. Adv Sci (Weinh). 2022;9:e2104106.
71. Liu C, Wu J, Li M, Gao R, Zhang X, Ye-Lehmann S, Song J, Zhu T, Chen C. Smad7 in the hippocampus contributes to memory impairment in aged mice after anesthesia and surgery. J Neuroinflammation. 2023;20:175.
72. Wang S, Lai X, Deng Y, Song Y. Correlation between mouse age and human age in anti-tumor research: significance and method establishment. Life Sci. 2020;242:117242.
73. Shimoda R, Amaya Y, Okamoto M, Soya S, Soya M, Koizumi H, Nakamura K, Hiraga T, Torma F, Soya H. Accelerated fear extinction by regular light-intensity Exercise: a possible role of hippocampal BDNF-TrkB signaling. Med Sci Sports Exerc. 2024;56:221–9.
74. Cazorla M, Premont J, Mann A, Girard N, Kellendonk C, Rognan D. Identification of a low-molecular weight TrkB antagonist with anxiolytic and antidepressant activity in mice. J Clin Invest. 2011;121:1846–57.
75. Han R, Liu Z, Sun N, Liu S, Li L, Shen Y, Xiu J, Xu Q. BDNF alleviates Neuroinflammation in the Hippocampus of type 1 Diabetic mice via blocking the aberrant HMGB1/RAGE/NF-kappaB pathway. Aging Dis. 2019;10:611–25.
76. Qin T, Guo L, Wang X, Zhou G, Liu L, Zhang Z, Ding G. Repetitive transcranial magnetic stimulation ameliorates cognitive deficits in mice with radiation-induced brain injury by attenuating microglial pyroptosis and promoting neurogenesis via BDNF pathway. Cell Commun Signal. 2024;22:216.
77. Jaudon F, Albini M, Ferroni S, Benfenati F, Cesca F. A developmental stage- and Kidins220-dependent switch in astrocyte responsiveness to brain-derived neurotrophic factor. J Cell Sci. 2021;134:jcs258419.
78. Niu C, Yue X, An JJ, Bass R, Xu H, Xu B. Genetic dissection of BDNF and TrkB expression in glial cells. Biomolecules. 2024;14:91.
79. Cui Y, Su D, Zhang J, Lam JST, Cao S, Yang Y, Piao Y, Wang Z, Zhou J, Pan H, Feng T. Dopaminergic versus anticholinergic treatment effects on physiologic complexity of hand tremor in Parkinson's disease: a randomized crossover study. CNS Neurosci Ther. 2024;30:e14516.
80. Di Liberto V, Borroto-Escuela DO, Frinchi M, Verdi V, Fuxe K, Belluardo N, Mudo G. Existence of muscarinic acetylcholine receptor (mAChR) and fibroblast growth factor receptor (FGFR) heteroreceptor complexes and their enhancement of neurite outgrowth in neural hippocampal cultures. Biochim Biophys Acta Gen Subj. 2017;1861:235–45.

Publisher's note